Phosphate Ester Hydrolysis in Aqueous Solution: Associative versus Dissociative Mechanisms

Jan Florián and Arieh Warshel*

Department of Chemistry, University of Southern California, Los Angeles, California 90089-1062

Received: July 3, 1997; In Final Form: October 6, 1997

Phosphate hydrolysis plays a major role in many biological processes. To fully understand such processes, it is essential to obtain a quantitative description of the corresponding reactions in solution. Here we present a systematic theoretical study of the nonenzymatic hydrolysis of monomethyl phosphate via the nucleophilic attack at the phosphorus center and explore the energetics of various reaction mechanisms as well as the structures and charge distributions of corresponding reaction intermediates and transition states. We consider all the relevant protonation states of the phosphate oxygens and two forms of the nucleophile that correspond to hydrolysis by OH^- and by neutral water. These systems are studied by using ab initio quantum mechanical calculations coupled with the Langevin dipoles (LD) and polarized continuum (PCM) solvation models. The reliability of the calculations is verified by comparing calculated and observed values of key reaction free energies, activation free energies, and kinetic isotope effects. Combining the calculated and observed information provides "consensus" free-energy surfaces for the hydrolysis of phosphate monoesters. It is found that the barriers for the associative pathways are similar to that of the dissociative pathways. Thus an enzyme active site could select either of these mechanisms depending on the particular electrostatic environment.

1. Introduction

Chemical reactions that involve the formation or cleavage of PO bonds in phosphate esters are of crucial importance in biochemistry. Over five decades, the determination of the dominant mechanism for these reactions in aqueous solution has been the subject of enormous experimental effort (see for example refs 1, 2 and references therein). Despite that, considerable uncertainty about the actual mechanism still remains. In particular, there is significant controversy about whether phosphate hydrolysis occurs through associative or dissociative mechanisms.

The reaction mechanisms that lead to the cleavage of the phosphoester bond can be divided in two major classes. Those mechanisms that proceed via the hydrated PO_3^- anion (metaphosphate) are called dissociative (Figure 1), whereas mechanisms that require formation of an intermediate or transition state with pentacovalent phosphorus (phosphorane) belong to the family of associative mechanisms (Figure 2).[3] Besides the availability of dissociative and associative pathways, the hydrolysis of phosphate esters is largely complicated by the possible involvement of either neutral, monoanionic, or and dianionic phosphate esters as substrates. Furthermore, these substrates can be attacked by either H_2O and OH^- nucleophiles (Figure 2).[4] Whereas mechanisms involving differently charged phosphates can be partially distinguished by measuring the pH dependence of the reaction kinetics, kinetic experiments cannot distinguish between a neutral water attack and steps involving proton transfer from water to the phosphate followed by a nucleophilic attack of the remaining OH^- on the phosphorus.

In some cases one can use experimental information about the stereochemistry of the reactants and products to determine whether the hydrolysis of phosphate esters in aqueous solution proceeds via associative or dissociative mechanistic pathways. However, such experiments are very difficult, as they must involve preparation of chiral phosphates by the stereospecific substitution of ^{16}O oxygen atoms by the ^{17}O and ^{18}O isotopes. After resolving the difficulties associated with the detection of very small chirality of such isotopically substituted phosphate esters, Buchwald et al. observed inversion of the configuration on phosphorus for aqueous alcoholysis of phenyl phosphate monoanion and 2,4-dinitrophenyl phosphate dianion.[5] Although this finding is directly indicative of an associative pathway, the authors concluded that "the actual mechanism is constrained to a preassociative pathway, in which the reversibly dissociating substrate only yields product in the presence of an acceptor nucleophile". This conclusion implies a somewhat concerted dissociative mechanism. In similar stereochemical experiments, racemization at phosphorus was observed for *tert*-butyl alcoholysis of phosphate monoesters in *tert*-butyl alcohol[6] and acetonitrile.[7] These experiments were interpreted as evidence for the dissociative reaction mechanism. However, the properties of the solvents used in these studies are markedly different from the corresponding properties of aqueous solution. Moreover, since the pentacovalent intermediate can possibly undergo ligand reorganization (pseudorotation) leading to the racemized

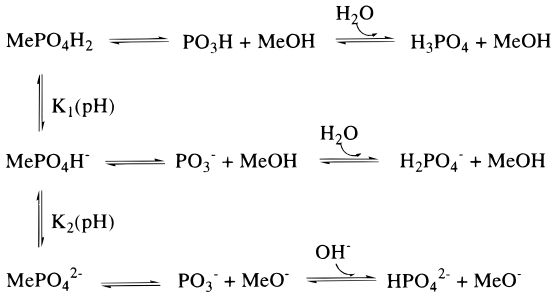

Figure 1. Pathways for dissociative hydrolysis of methyl phosphate. Symbols Me and *K*(pH) denote, respectively, methyl groups and pH-dependent equilibrium constants.

S1089-5647(97)02182-2 CCC: $15.00
Published on Web 01/22/1998

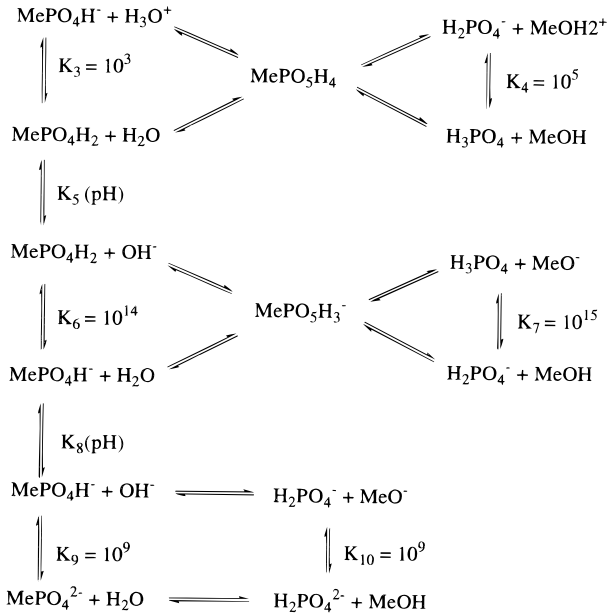

Figure 2. Pathways for associative hydrolysis of methyl phosphate. Symbols Me, *K*, and *K*(pH) denote, respectively, methyl groups, equilibrium constants, and pH-dependent equilibrium constants.

product,[8] the associative mechanism cannot be uniquely excluded only on the basis of the observed racemization. Besides stereochemical methods, the mechanism of the given reaction can be studied indirectly by measuring rates of hydrolysis for differently substituted substrates and by interpreting these rates using linear free energy relationships (LFER). However, this methodology involves several assumptions, which are not fully justified. This includes, for example, the assumption that the actual reaction mechanism is not affected by changes in the substrate structure. Furthermore, the interpretation of the observed LFER is far from being unique and can be rationalized by different alternative mechanisms (see the discussion section and ref 9). Finally, the measurement of the reaction rates for the P−O(C) bond cleavage is often hampered by competing reactions that involve substitutions at the carbon atom.

Ab initio methods combined with reliable solvation models can in principle augment experimental studies and help in overcoming some of the limitations outlined above. Namely, such approaches can help in determining the activation energies and the corresponding rate constants for individual reaction mechanisms as well as geometries and charge distributions of the corresponding transition states and unstable intermediates. Early ab initio calculations of PO bond cleavage in phosphate esters were reported by Gorenstein and co-workers,[10,11] who calculated gas-phase reaction profiles for the associative mechanism in base-catalyzed hydrolysis of gauche−gauche and gauche−trans conformers of the dimethyl phosphate anion, and by Hayes, Kenyon, and Kollman,[12] who examined the thermodynamics of hydrolysis for various phosphate esters and anhydrides. Although these calculations pointed out the importance of stereoelectronic and solvation effects, they could not provide the quantitative information needed for mechanistic studies. These nonquantitative results reflected the use of small basis sets, partial geometry optimizations, and unparametrized spherical-cavity continuum solvation models. The ab initio methodology was significantly upgraded in subsequent theoretical studies,[13−17] but solvation effects were not considered in these calculations. The free energy barriers that involved solvation contributions were reported only for the OH^- attack on ethylene phosphate[18,19] and mono,[4] di-,[18,19] and trimethyl[4] phosphate. Except for our recent study[4] that questioned the validity of some of the strongest evidence for dissociative mechanisms, previous theoretical studies did not address the important question of the actual reaction mechanism, but focused on the existence of dianionic phosphorane intermediates[13−16] the role of strain,[18,19] and the isomerization of $PO_3^-\cdot(H_2O)_n$ clusters to $H_2PO_4^-\cdot(H_2O)_{n-1}$.[20] At any rate, it seems to us that ab initio methods with properly calibrated solvation models have reached the stage where they can provide useful insights into the energetics and mechanism of phosphate hydrolysis in solution. Here we report such a theoretical study based on MP2/6-31+G(d,p) and HF/6-31G(d) ab initio quantum mechanical calculations coupled to the Langevin dipoles (LD) and polarized continuum (PCM) solvent models.

2. Methods

To study the energetics of chemical reactions in solution, it is essential to incorporate solvation effects in a quantitative way. Several approaches are capable of performing this task.[21−31] Here we deal with a case where the relevant energetics are not fully available from experimental studies, and one has to rely on high-level ab initio calculations and on a well-calibrated solvation model. Thus, we use as our primary tool the recent version of the Langevin dipoles (LD) model that has been carefully calibrated for calculation of hydration free energies of both neutral and ionic solutes.[32] Other well-calibrated solvent models are expected to provide similar results. The actual implementation of our approach is described below.

2.1. Gas-Phase Calculations. The present work used gas-phase geometries as a starting point for geometry search in solution (see section 2.4). The gas-phase geometries of the reactants, products, and transition states (TSs) were calculated by the gradient optimization at the Hartree−Fock (HF)/6-31G-(d) level. The characteristics of all stationary points as well as zero-point vibrational energies (ZPEs) were evaluated by subsequent calculations of the HF/6-31G(d) harmonic vibrational frequencies. The gas-phase energies were determined for the HF/6-31G(d) geometries by using the second-order Møller−Plesset perturbation theory (MP2) and the 6-31+G(d,p) basis set.

Gas-phase reaction coordinates were evaluated using the intrinsic reaction coordinate (IRC) approach.[33,34] This calculation involved the determination of the steepest descent path from the TS toward the reactant and product state. The IRC calculations were carried out at the HF/6-31G(d) level, and the first step from the TS geometry was made along the normal mode corresponding to the negative eigenvalue of the Hessian (second energy derivative) matrix. The reaction coordinates were computed in mass-weighted internal coordinates (step size 0.1 $amu^{1/2}$ bohr) by using the method of Gonzales and Schlegel.[35] All ab initio calculations were carried out with the Gaussian 94 program.[36]

2.2. Solvation Free Energies. Solvation free energies (related to the free energy of transfer of the solute molecule from the 1 M vapor to 1 M aqueous solution at 298 K) were calculated by using the Langevin dipoles (LD) model of the solvent.[22,32,37,38] For the sake of comparison, solvation free energies were also calculated by using the polarized-continuum model (PCM) of Miertus, Scrocco, and Tomasi.[39,40] Default Pauling's atomic radii[41] multiplied by a standard factor of 1.2[23,40] and a dielectric constant $\epsilon = 80$ were used for the PCM calculations. The LD and PCM calculations were carried out for the gas-phase HF/6-31G(d) structures of the stationary points by using the programs ChemSol 42 and Gaussian 94.[36] The

effects of electron correlation and solvation energies on transition state geometries were studied systematically wherever it was suspected that such effects could be important. This was done by evaluating single-point MP2/6-31+G(d,p) energies and solvation energies along the entire reaction coordinate (see section 2.4).

The LD solvation model evaluates an average polarization of the solvent molecules surrounding the solute by using a discrete dipolar representation of the solvent. This model is parametrized to reproduce experimental solvation free energies of a representative set of small neutral and ionic molecules. Here we used the recent iterative version of this model (ILD), which was developed and refined for studies of solvation effects in aqueous solutions.[32] This model uses potential-derived HF/6-31G(d) and MP2/6-31+G(d,p) atomic charges to represent the charge distribution of the solute molecules. The energy contributions associated with the polarization of the solute by the solvent (solute induction effects) are evaluated using the solute charges evaluated by the PCM model.[39,40] In addition to the electrostatic and induction contributions, the calculated LD solvation free energy involves parametrized terms that represent dispersion and hydrophobic solute−solvent interactions. Except for the oxygen atoms of H_2O and OH^-, the van der Waals (vdW) radii and other parameters of the LD model used in this study were the same as in the general parametrization described previously.[32] The vdW radius of the oxygen atom of H_2O and OH^- was treated as a linear function of the distance to the phosphorus atom along the reaction coordinate. This vdW radius attained the limiting values of 2.35 Å (oxygen in H_2O and OH^-) and 2.8 Å (inorganic oxygen) for PO distances of 2.8 and 1.64 Å, respectively.

2.3. Activation Barriers and Reaction Free Energies. Our task is to evaluate activation free energies and reaction free energies for the reactions considered. In studies of reactions in solution we deal with the enormous dimensionality of the solute−solvent system. Therefore, the relevant free energies are evaluated in terms of the corresponding potential of mean force (PMF), which is obtained by fixing one or two coordinates (reaction coordinates) and averaging over the rest of the coordinates (see, for example, ref 43). Although more rigorous treatments of chemical reactions in solutions should take nonequilibrium solvation effects into account,[44,45] one can use the PMF to estimate the activation free energy ($\Delta G^{\ddagger}$) and the rate constant (k). This can be done using the relationships (see, for example, ref 45)

$$k = \tau^{-1} \exp(-\Delta G^{\ddagger}\beta) \tag{1}$$

where $\beta = (k_B T)^{-1}$ (k_B and T are the Boltzmann constant and temperature, respectively) and τ is the time it takes for a reactive trajectory to cross the transition state region, $\Delta x^{\ddagger}$. The value of $\Delta x^{\ddagger}$ is usually determined by the relationship

$$\Delta g(x^{\ddagger}) - \Delta g(x^{\ddagger} - \Delta x^{\ddagger}/2) = \beta^{-1} \tag{2}$$

Here, $\Delta g(x)$ is the above-mentioned PMF and $x^{\ddagger}$ is the value of the reaction coordinate at the transition state. The value of τ^{-1} is quite similar for many types of reactions in condensed phases and can be approximated at room temperature by

$$\tau^{-1} \cong 6 \times 10^{12}\ \mathrm{s}^{-1} \tag{3}$$

Note that the activation free energy $\Delta G^{\ddagger}$ is obtained from the PMF through the relationship

$$\exp\{-\Delta G^{\ddagger}\beta\} = \exp\{-\Delta g^{\ddagger}\beta\}(\Delta x^{\ddagger}/\int_{-L}^{x^{\ddagger}} \exp\{-\Delta g(x)\beta\}\mathrm{d}x) \tag{4}$$

Here, the integration limit is not taken as infinity but rather the radius L ($L \approx 7$ Å) of a solvent sphere that contains one molecule of each reactant in a concentration of 1 M. In this way[45] we automatically deal with a standard state. Finally, the reaction free energy is given by

$$\exp\{-\Delta G^{0}_{a\rightarrow b}\beta\} = (\int_{x^{\ddagger}}^{L} \exp\{-\Delta g(x)\beta\}\mathrm{d}x)/(\int_{-\mathrm{L}}^{x^{\ddagger}} \exp\{-\Delta g(x)\beta\}\mathrm{d}x) \tag{5}$$

In principle, one should evaluate the free energy surfaces for chemical reactions in solution by rigorous combination of free energy perturbation (FEP)/umbrella sampling approaches (see, for example, refs 44, 45). These surfaces can be considered as the above PMFs, although they are somewhat more rigorous, as they reflect nonequilibrium solvation effects. However, such calculations are very challenging when performed with ab initio solute surfaces.[46] Thus it is important to obtain a practical approximation to the FEP approach. The approximation we use here (related previous studies date back to 1979[22]) represents the reaction PMF by

$$\Delta g(x) = g(x) - g(x_0) = \Delta U_{\mathrm{solute}}(x) + \Delta\Delta G_{\mathrm{solv}}(x) + \Delta ZPE\lambda(x) - \alpha T\Delta S'_{\mathrm{solute}}\lambda(x) \tag{6}$$

where x is the reaction coordinate, x_0 is a reference value of the coordinate (e.g. x_0 can be taken as infinity or the minimum of PMF), $\Delta g(x)$ is the PMF, $\Delta U(x)$ is the change in the solute potential energy as a function of x and $\Delta\Delta G_{\mathrm{solv}}(x)$ is the change of the solvation free energy. $\Delta S'$ and ΔZPE are, respectively, the changes in the gas-phase entropy and zero-point energy of the solute upon going from the reactant state (x_0) to the transition state or another stationary point. These values are given for a state of 1 M concentration. α is a scaling constant and $\lambda(x)$ is an interpolation coefficient that changes linearly from 0 to 1 between x_0 and the transition state or the intermediate for which $\Delta S'$ is evaluated. $\Delta S'$ includes only two-thirds of the actual solute translational entropy since one degree of freedom is converted to the reaction coordinate and the corresponding free energy is recovered by the integration of the PMF of eq 4. This approximation considers $\Delta S'$ for chemical reactions of charged molecules in solution and tries to account for solvent compensation effects and for the fact that molecular complexes and transition states are much more floppy in solution than in the gas-phase (e.g., TS1 in section 3.2). This is done by the scaling factor α, which is usually taken as zero, but estimates of the solute entropic contributions with larger α values (e.g., $\alpha = 0.5$) might be useful. The approximation of eq 6 was found to work quite well in previous LD studies that used experimental gas-phase enthalpies and solvation free energies (e.g., refs 22, 47). This reflects, in part, the fundamental physics of compensation effects and to some extent the fact that our solvation free energies were calibrated on thermodynamic cycles that involve reaction free energies (and were perhaps forced to compensate for the corresponding solute entropies). Thus it will be important to examine the basis of our approximation by a careful comparison of rigorous FEP results to those obtained with the present approach. In some simple cases, such as S_N2 reactions, we find that the LD and FEP approaches give similar results. However, the convergence of entropic calculations in FEP is still rather poor, particularly in studies of bond formation processes, and more studies are needed. We also note that the

TABLE 1: Comparison of the Calculated and Observed Reaction Free Energies (kcal/mol)

no.	reaction	ΔE_{MP2}[a]	ΔZPE[b]	$\Delta\Delta G_{LD}$[c]	$\Delta\Delta G_{PCM}$[d]	$T\Delta S'$tr[e]	$T\Delta S'$[f]	Δg[g]	$\Delta G°_{calc}$[h]	$\Delta G°_{exp}$[i]
1	$MeOPO_3H_2 + H_2O \rightleftharpoons MeOPO_3H_3^+ + OH^-$	186.8	−1.8	−156.7	−169.4	0.0	−0.8	28.3	27.3	25.5 ± 3.0[j]
2	$MeOPO_3H^- + H_2O \rightleftharpoons MeOPO_3H_2 + OH^-$	63.5	−1.4	−41.8	−47.0	0.0	−0.1	20.3	19.3	19.5 ± 0.5
3	$MeOPO_3^{2-} + H_2O \rightleftharpoons MeOPO_3H^- + OH^-$	−63.2	−0.4	73.6	77.9	0.0	−1.0	10.0	9.0	12.5 ± 0.5
4	$PO_4H_3 + MeOH \rightleftharpoons PO_4H_4^+ + MeO^-$	188.8	−3.0	−151.0	−161.1	0.0	−0.7	34.8	34.8	25.0 ± 3.0[k]
5	$PO_4H_2^- + MeOH \rightleftharpoons PO_4H_3 + MeO^-$	60.7	−2.9	−32.5	−32.3	0.0	−0.5	25.3	25.3	19.0 ± 0.5
6	$PO_4H^{2-} + MeOH \rightleftharpoons PO_4H_2^- + MeO^-$	−68.6	−2.2	84.3	94.5	0.0	−1.1	13.5	13.5	12.1 ± 0.5
7	$MeOPO_3H_2 + H_2O \rightleftharpoons PO_4H_3 + MeOH$	3.1	0.8	0.7	0.3	0.3	0.2	5.0	4.0	−3 ± 1
8	$MeOPO_3H^- + H_2O \rightleftharpoons PO_4H_2^- + MeOH$	2.1	1.0	1.9	0.5	0.3	0.6	4.6	3.6	−2 ± 1
9	$MeOPO_3^{2-} + H_2O \rightleftharpoons PO_4H^{2-} + MeOH$	3.7	1.5	1.7	−1.2	0.3	0.7	6.9	5.9	−0.7 ± 1
10	$MeOPO_3H^- + H_2O \rightleftharpoons MeOPO_4H_3^-$	12.0	3.6	12.3	10.0	−5.5	−7.1	27.9	29.3	25 ± 4
11	$MeOPO_3H_2 + H_2O \rightleftharpoons MeOPO_4H_4$	−1.7	3.7	13.5	9.3	−5.5	−7.8	15.5	16.9	16 ± 3
12	$MeOPO_3H_2 \rightleftharpoons PO_3H + MeOH$	46.1	−1.6	−5.1	−3.7	5.7	6.7	38.4	36.0	29[l]
13	$MeOPO_3H^- \rightleftharpoons PO_3 + MeOH$	29.7	−1.9	−1.3	−2.2	5.7	6.3	26.5	24.1	25 ± 3
14	$MeOPO_3H^- \rightleftharpoons PO_3H + MeO^-$	105.7	−4.2	−36.4	−35.8	5.7	6.6	65.1	62.7	49[l]
15	$MeOPO_3^{2-} \rightleftharpoons PO_3^- + MeO^-$	−37.3	−3.6	82.8	90.6	5.7	5.3	41.9	39.5	37 ± 3
16	$PO_4H^{2-} \rightleftharpoons PO_3^- + OH^-$	−37.1	−3.8	70.6	76.9	5.4	4.6	29.7	27.3	36 ± 2
17	$PO_4H_2^- \rightleftharpoons PO_3^- + H_2O$	27.7	−2.8	−3.2	−2.7	5.5	5.7	21.7	20.3	27 ± 2

[a] Difference in the MP2/6-31+G**//HF/6-31* energies (products − reactants). [b] Difference in the HF/6-31G* zero-point vibrational energies of products and reactants, scaled by 0.9. [c] Difference in the LD solvation free energies of products and reactants. [d] Difference in the PCM solvation free energies of products and reactants. [e] $\Delta S'_{tr}$ denotes the change in translational entropy during the reaction, evaluated for 1 M ideal gas and scaled by 2/3 (see section 2.3). The temperature is taken as T = 298 K. [f] $\Delta S'$ was taken as the sum of $\Delta S'_{tr}$ and the change in rotational and vibrational entropy during the reaction for 1 M ideal gas. [g] $\Delta g_{calc} = \Delta E_{MP2} + \Delta ZPE + \Delta G_{LD} - \alpha T\Delta S'$, where $\alpha = 0$ (see section 2.3). [h] Calculated by using eq 5, with the numerical estimates for the free energies required to transfer the reactants and products from 1 M solution to a contact distance as explained in section 2.3. [i] The $\Delta G°_{exp}$ values for proton-transfer reactions were obtained from experimental pK_a differences.[51] For other reactions, $\Delta G°_{exp}$ values for monoethyl phosphates estimated by Guthrie[51] are given. Standard states are 1 M aqueous solution and pure liquid (55 M H_2O) at 25 °C and 1 atm. See also the text. [j] Assuming the value of −2.9 for the pK_a constant of $MeOPO_3H_3^+$.[51] [k] Assuming the value of −2.3 for the pK_a constant of $PO_4H_4^+$.[51] [l] Estimated by assuming the pK_a constant of PO_3H to be equal to pK_a for nitric acid (−1.4).[51]

solute entropy cannot be easily determined experimentally since the observed entropic effects include the contributions of the solvent. Thus in the absence of more unique information we prefer to use the somewhat ad hoc relationship of eq 6 with a small α value. In doing so we consider the effect of changing α from 0 to 0.5 as a possible error range, which is usually less than 5 kcal/mol. We also note that using the unscaled gas-phase solute entropies frequently gives results that are in clear conflict with experimental free energy differences in solution (see Table 1).

In implementing eq 6 we take $\Delta U(x)$ as the MP2/6-31+G-(d,p) energy differences and determine the $\Delta G_{solv}(x)$ values by the LD and PCM models (as described in section 2.2). The ΔZPE term is calculated from the HF/6-31G(d) harmonic vibrational frequencies multiplied by the factor 0.9, and $\Delta S'$ is evaluated as a sum of the translational (two-thirds of the total effect), rotational, and vibrational ideal gas contributions at 1 M concentration.[43] The PMF of eq 4 has to describe the corresponding free energy in the entire volume considered. Fortunately, the PMF in the range between infinity and the contact region can be approximated by

$$\Delta g(x) = \Delta U(x)/\epsilon_{eff} \qquad (7)$$

where $\epsilon_{eff} \geq 30$. This approximation was found to describe quite reliably the interaction between charged molecules in solution[47] and is the basis for the current success of the so-called generalized Born model (see, for example, ref 24 and the discussion in Appendix A of ref 48). Equation 7 can be further approximated to within 2 kcal/mol by assuming that $\Delta g(x)$ is constant. The actual implementation of quantum mechanical molecular calculations in studies of complex reactions forces one to consider conceptual difficulties that are not familiar to many workers in the field. That is, physical organic chemists usually discuss reaction kinetics in terms of concentration rather than in terms of PMF. This is, of course, fully consistent with the laws of kinetics and thermodynamics, but it does not help in relating ab initio potential surfaces to observed kinetic parameters. Trying to accomplish such a task while talking about effective concentration can become quite complicated (and sometimes hopelessly confusing). The situation is particularly complicated when one deals with reactants of different concentration (i.e., OH^- and H_2O) or with enzymatic reactions. An effective way of using well-defined molecular potential surfaces and the corresponding PMF while avoiding the complications associated with concentration effects was proposed in ref 49. This and other related works (see, for example, ref 45) suggested considering the PMF in a solvent cage where all the reactants are already packed together and evaluating the rather trivial concentration effect separately. In doing this, we note that the effect of bringing the relevant reactants from 1 M concentration to the solvent cage is easily estimated assuming that the $\Delta g(x)$ of eq 7 is approximately constant (see above). This gives

$$\Delta G(1\text{ M}\rightarrow\text{cage}) \approx -RT\ln(\Delta x_0/L) \approx 1\text{ kcal/mol} \qquad (8)$$

where Δx_0 is the region within the cage where the change in Δg is less than β^{-1}. Here we assume that $\Delta x_0 \approx 1$ Å and use $L = 7$ Å. This result is, of course, similar to the result obtained for changing the concentration from 1 M to 55 M. With the above considerations we have to correct activation barriers that involve the attack of OH^- by

$$\Delta G^{\ddagger}(OH^-)_{1M} \approx \Delta G^{\ddagger}(OH^-)_{PMF} + 1\text{ kcal/mol} \qquad (9)$$

This treatment does not include, of course, the OH^- generated during the attack by water since the water molecules are always present in the solvent cage. The calculation of $\Delta G^{\ddagger}_{PMF}$ is acomplished by using eq 4. In doing so we use $\Delta x^{\ddagger} \approx 0.1$ Å and $\Delta x_0 \approx 1$ Å. This gives

$$\Delta G^{\ddagger}_{PMF} \approx \Delta g^{\ddagger} + 1.4\text{ kcal/mol} \qquad (10)$$

2.4. Geometry Search along the Reaction Coordinate in Solution. The present work focuses on the energetics of

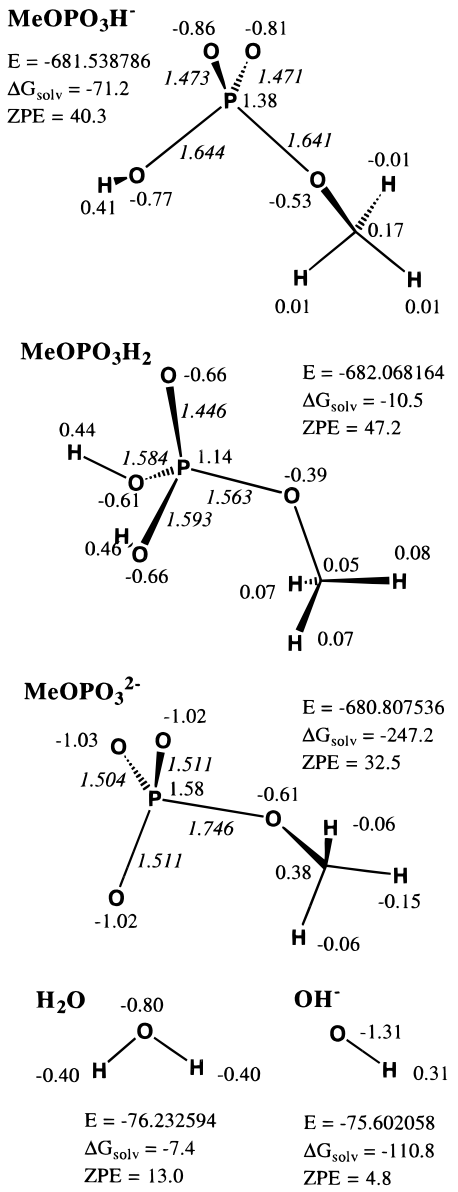

Figure 3. Structures of the possible reactants in the hydrolysis reaction of methyl phosphate. The bond lengths (Å) and the potential-derived MP2/6-31+G(d,p) atomic charges (gas-phase, au) are given as italic and roman numbers, respectively. *E*, ZPE, and ΔG_{solv} denote MP2/6-31+G(d,p) energy (au), scaled HF/6-31G(d) zero-point energy (kcal/mol), and LD solvation free energy (kcal/mol), respectively.

phosphate hydrolysis in solution rather than on determining the exact transition-state structure, which is somewhat less crucial for understanding reaction rates (transition-state surfaces in solutions are frequently rather flat). To explore the free energy surface near each TS, we performed a search along the gas-phase intrinsic reaction coordinate (IRC) and determine the corresponding free energy in solution (eq 6) as a function of this parameter. The calculated IRCs usually contained a sequence of 80−160 geometries. These data allow us to explore the free energy in solution along the gas-phase minimum energy path from the TS to the corresponding reactant and product valleys. Searches in other dimensions were also performed (see below). The separate LD, PCM, and MP2/6-31+G(d,p) calculations were carried out typically for every fifth point of each IRC. Because the distances from the phosphorus atom to the attacking and leaving groups contribute dominantly to the gas-phase IRC coordinates, we were able to estimate the change of the P−O(H) and P−O(Me) bond lengths upon going from the

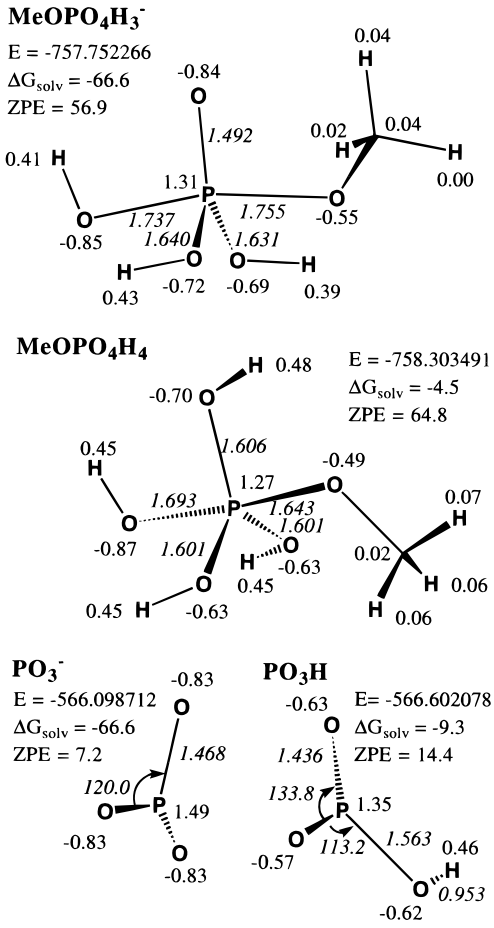

Figure 4. Structures of possible intermediates in the hydrolysis reaction of methyl phosphate. For explanation of various numerical values see the legend to Figure 3.

gas-phase to aqueous solution. Naturally, using the one-dimensional IRC for two-dimensional mapping is not fully general, and it reflects the assumption that the P−O(H) and P−O(Me) coordinates are coupled in a similar way in gas-phase and solution. This assumption is reasonable since the bond length to the leaving group is expected to gradually increase as the attacking nucleophile approaches more closely the phosphorus atom in both solution and gas-phase. As far as the solvation effects on the proton transfer to and from the phosphate group are concerned, we noted that electron correlation and solvation energies tend to compensate each other in modulating the barrier height and position. This compensation effect involves about 2 kcal/mol uncertainty and does not affect significantly the overall energetics of phosphate ester hydrolysis. Similarly, the contributions of solvent-induced conformational changes to the overall energetics can be safely neglected. Finally, in cases where the solvation effects upon a perpendicular coordinate were identified as essential (for example the coupling between the P−O(H) and P−O(Me) distances and the orientation of the equatorial (P)O−H bond in the configurational region of dianionic phosphorane) we searched the free energy surface manually.

3. General Results

3.1. Equilibrium Properties. The gas-phase structures of the reactants, reaction intermediates, and products considered in this study are depicted in Figures 3−5. These coordinates provided the starting point for our solution geometry search, and in many cases they do not change significantly in solution.

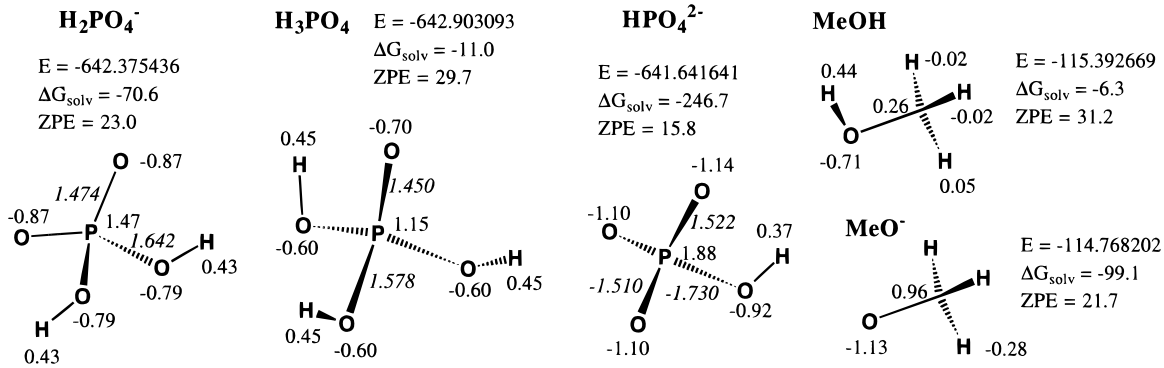

Figure 5. Structures of possible products in the hydrolysis reaction of monomethyl phosphate. For explanation of notation and energy values see the legend to Figure 3.

TABLE 2: Gas-Phase Energy Change for the Reaction $MeOPO_3H^- + H_2O \rightleftharpoons PO_4H_2^- + MeOH$, Calculated at Various Levels of Theory

method[a]	ΔE[b]	ΔZPE[c]
HF/6-31G(d)	−0.7	1.0
HF/6-31+G(d,p)//A	−0.7	
HF/6-311++G(2d,p)//A	−0.9	
HF/6-311++G(2d,p)//B	−1.0	
MP2/6-31+G(d,p)//A	2.1	
MP2/6-31+G(d,p)	2.2	1.0
MP2/6-311++G(2d,p)//B	1.9	
MP4[d]//6-311++G(2d,p)//B	1.3	

[a] Energy//geometry. The computational methods used for the geometry optimization are denoted as follows: A = HF/6-31G(d), B = MP2/6-31+G(d,p). [b] Difference in total gas-phase energies (i.e., electronic energy and nuclei repulsion), $\Delta E = E_{products} - E_{reactants}$, in kcal/mol. [c] Difference in zero-point vibrational energies (products − reactants) in kcal/mol. [d] MP4(SDQ), frozen core.

For pentavalent phosphorane intermediates, the methoxy group was always assumed to occupy the axial position, as PO bond cleavage is generally considered to be more feasible for axially oriented leaving groups. Indeed, the bond lengths of axial PO bonds were calculated to be about 0.1 Å longer than for the corresponding equatorial groups in both the neutral and monoanionic phosphorane intermediates (Figures 3−5). Except for the position dependence, the length of the P−O(H) and P−O(Me) bonds are strongly affected by the total molecular charge. The shortest P−O(H) and P−O(Me) bond lengths were found in neutral monomethyl phosphates and phosphoranes. This trend reflects stronger covalent bonding in neutral species. Conversely, the differences in charges on the phosphorus and oxygen atoms (bond polarities) increase upon deprotonation (Figures 3−5).

The calculated free energy changes for methyl phosphate hydrolysis in aqueous solution and related processes are compared with available experimental data in Table 1. The first set of reactions (1−6) involve proton-transfer equilibria. The free energies for these reactions involve compensations between large gas-phase and solvation energies. Therefore, the 5 kcal/mol accuracy of the calculated proton-transfer free energies is considered here as an encouraging result that confirms viability of our MP2+LD computational methodology, as well as the validity of eq 6. The replacement of the LD solvation energies by the PCM solvation energies results in larger disagreement with the experimental data for reactions that involve dianions. Table 1 also gives the calculated entropic contributions to the gas-phase free energy. These entropic contributions can be used to estimate the error range associated with the use of α in eq 6. The results for reactions 10−17 illustrate the point of section 2.3 that one should not use unscaled gas-phase entropies in calculating PMFs for solution reactions.

For the enzymatic hydrolysis of monoethyl phosphate in aqueous solution at pH 7.3, enthalpy changes of 0 ± 0.2 kcal/mol were observed for both mono- and dianionic species.[50] Measurements of the free energy changes for the hydrolysis reactions of phosphate monoesters have not been reported, perhaps because the slow reaction rates made it hard to reach equilibrium in a reasonable time scale or because these thermodynamic data have not been viewed as a useful way of resolving mechanistic issues. The crucial importance of quantitative analysis of the energetics of phosphate ester hydrolysis reactions was realized by Guthrie[51] who corrected experimental enthalpies of Gerlt et al.[50] for heats of protonation and estimated the corresponding entropy change by using Benson's bond-contribution method.[52] Guthrie's results are compared with our calculated values in Table 1 (reactions 7−9). Since the differences between our and Guthrie's free energies for these reactions amount to ∼7 kcal/mol and both LD and PCM methods provide similar solvation contributions, we examined in detail the sensitivity of the calculated gas-phase energetics to the applied computational level. Here we were especially concerned about possible errors associated with the use of geometries optimized at the HF/6-31G(d) level. However, the energies obtained for the geometries optimized at the MP2/6-31+G** level as well as MP2 energies obtained with the basis set of triple-ζ quality indicate only minimal geometry and basis set dependence of our results (Table 2). The electron correlation effects evaluated by the many-body perturbation theory of the fourth order (MP4) tend to destabilize products of this reaction by 2.3 kcal/mol. These effects are only slightly overestimated at the MP2 level. Thus, the MP2/6-31G+(d,p)//HF/6-31G(d) method used in this work can be considered to be sufficiently accurate. Similarly, the solvation free energies (ΔG_{solv}) of neutral solutes appear to have reasonable accuracy. For example, our LD ΔG_{solv} of water (−7.4 kcal/mol) and methanol (−6.2 kcal/mol) agree well with the corresponding experimental values[53,54] of −6.4 and −5.1 kcal/mol, respectively. The calculated differences in proton affinities and ΔG_{solv} between inorganic and methyl phosphates are small. This finding agrees with the relatively small differences in the pK_a's of inorganic and methyl phosphates. Unfortunately, reliable experimental gas-phase basicities and solvation free energies of ionic phosphates are not available. In summary, the correct free energies for hydrolysis reactions of phosphate ester are most probably close to 0 kcal/mol and lie between our values and those estimated by Guthrie.[51]

The thermodynamic data for reactions 10−17 (Table 1) quantify the energetics of high-energy intermediates such as

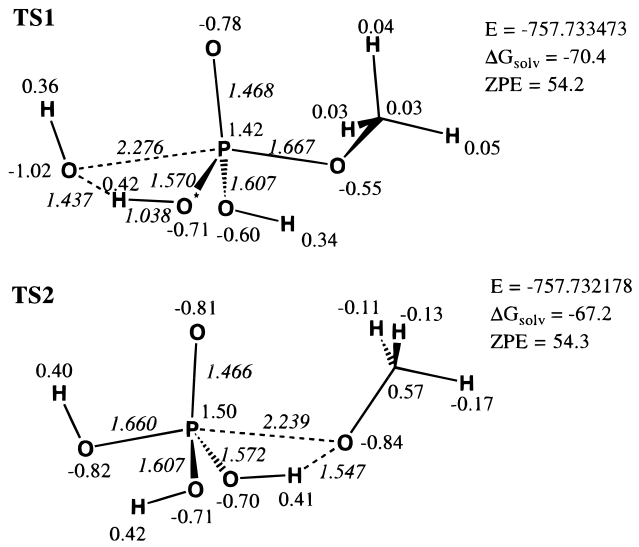

Figure 6. Structures of gas-phase transition states (TSs) for the associative hydrolysis of methyl phosphate. The TSs considered lead to the monoanionic pentavalent intermediate. For notation see the legend to Figure 3.

metaphosphate and phosphoranes. Our calculated results are in a reasonable agreement with the corresponding experimental estimates based on related kinetic and calorimetric data.[51]

3.2. Transition-State Properties and Reaction Coordinates. *3.2.1. Associative Mechanisms.* The gas-phase structures of transition states for the associative hydrolysis of monoanionic and neutral monomethyl phosphate are presented in Figure 6. These gas-phase structures were considered as the starting point for our solution studies. However, in the present case it was found that solvation effects have only negligible effect on the positions of these TSs along the reaction coordinate (as determined by evaluating solvation contributions along the whole reaction pathway; see below). Thus, we consider the gas-phase TS geometries as a reasonable representation for the corresponding structures in solution. Because of the larger gas-phase basicity of the hydroxide and methoxide ions compared to that of phosphate monoanions, transition structures in Figures 6 lie on reaction coordinates involving neutral water and methanol as reactants and products. The positions of the protons in TS1 (Figure 6) indicate that in the *neutral water attack on methyl phosphate monoanion* the proton-transfer step occurs before the TS is reached. This is confirmed by the calculated variations of the atomic positions along the intrinsic reaction coordinate (Figure 7). As a mechanistic consequence, the TS for the OH^- attack at the neutral monomethyl phosphate can be structurally similar to TS1. This structural similarity was confirmed by our evaluation of the reaction coordinate for the OH^- attack.[4] It is important to note that TS1 is expected to be quite floppy in solution since it involves several partially bonded fragments. This floppiness justifies our procedure for scaling $\Delta S'$ (see section 2.3). The geometry of TS2 exhibits features analogous to that of TS1 as the PO bond cleavage precedes the proton-transfer steps in the dissociation of the pentavalent intermediate into methanol and dihydrogen phosphate anion. Also for this partial reaction, the formation of the methoxide ion can be expected to be energetically accessible.

The free energy profile for the associative hydrolysis of methyl phosphate monoanion in aqueous solution is presented in Figure 8, along with the corresponding relative energies for the gas-phase reaction. The predicted increase in the activation barriers in solution originates from the fact that solvation stabilization of a monoanion is always smaller than the sum of

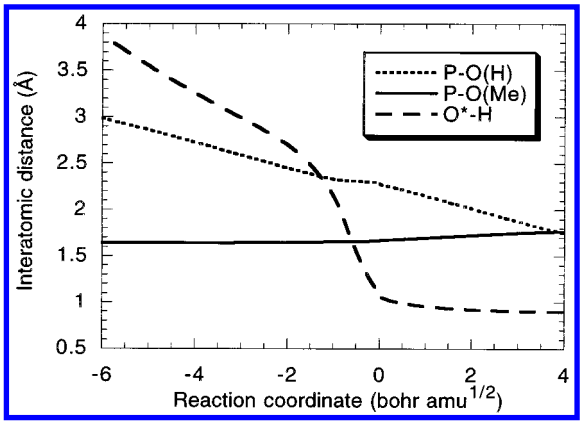

Figure 7. Variation of the axial PO bond lengths and the proton position along the intrinsic reaction coordinate originating from the TS1 structure (Figure 6). The TS1 structure corresponds to the zero value of the reaction coordinate.

solvation energies of its infinitely separated neutral and monoanionic fragments (reactants). The LD and PCM solvation free energy (ΔG_{solv}) contributions to the energetics of this reaction are compared in Figure 9. Because different atomic van der Waals radii were used in the PCM and LD calculations and, less importantly, because of the intrinsic differences in the modeling of the aqueous solvation, the LD and PCM solvation models provide quite different ΔG_{solv} values. However, the solvation contributions to the reaction kinetics and thermodynamics measured by the differences in ΔG_{solv} between reactants, transition states, and products are similar at both the LD and PCM levels.

As the infinitely separated reactants approach each other, the gas-phase energy decreases due to the formation of a hydrogen-bonded complex (for a detailed account of gas-phase hydration of ionic phosphates see the recent studies of Ma et al.[20] and Blades et al.[55] and references therein). The corresponding free energies in solution were not evaluated by us since they are similar to the free energies of reactants at infinite separation (see eq 7) and since the value of the PMF at the given TS is sufficient for estimating $\Delta G^{\ddagger}$. When the distance between the phosphorus and the nucleophilic oxygen (P−O(H)) becomes smaller than about 3 Å, the total energy of the complex steeply increases until TS1 (Figure 6) is reached. Interestingly, ΔG_{solv} remains approximately constant along this part of the reaction coordinate. A small bump (~2 kcal/mol) on the ΔG_{solv} profile was calculated for the part of the reaction coordinate that is dominated by the proton-transfer step. ΔG_{solv} increases in the region of the reaction intermediate and TS2, but this change is not large enough to change the positions of these stationary points on the reaction coordinate. Furthermore, it is highly improbable that the ΔG_{solv} term could change the geometric parameters related to the stiff degrees of freedom that are perpendicular to the reaction coordinate. Although solvation-induced conformational changes cannot be excluded, our conformational analysis of phosphate and phosphonate ester monoanions in aqueous solution[56] has shown that these free energy differences are small compared to the overall barrier for the hydrolysis reaction.

Knowledge of the changes in effective atomic charges during the reaction can be useful for estimating possible rate acceleration by external dipoles and charged groups, for example, the effects of enzyme active sites. Such charge variations can be estimated by comparing the data presented in Figures 3 and 6. The negative charge on the attacking oxygen atom increases

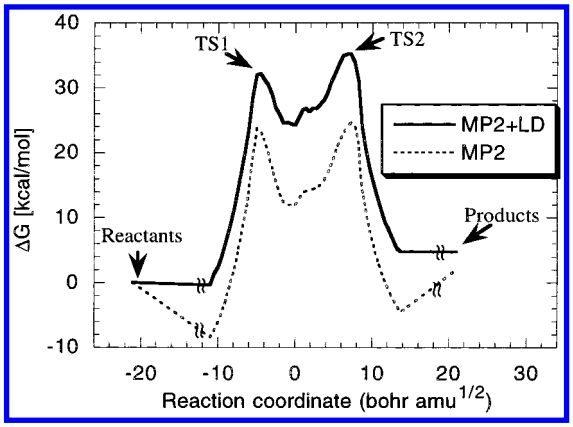

Figure 8. Comparison of the calculated energy and free energy profiles of the $H_2O + MeOPO_3H^- \rightleftharpoons H_2PO_4^- + MeOH$ reaction in the gas phase (MP2/6-31+G** energy differences, dotted line) and aqueous solution (LD + MP2/6-31+G** free energy differences, solid line). The geometries along the reaction coordinate were generated by two independent HF/6-31G* IRC calculations starting from the TS1 and TS2 structures (Figure 6). The origin of the reaction coordinate corresponds to the pentavalent intermediate, $MeOPO_4H_3^-$ (Figure 4). The IRC calculations were terminated for the geometries in which the distance between phosphorus and the oxygen of the attacking (leaving) group reached 2.98 Å (3.05 Å). These structures correspond to the reaction coordinates of −11.0 and 13.7 bohr amu$^{1/2}$, respectively. The reaction coordinates for reactants and products were incidentally chosen to be ±20 bohr amu$^{1/2}$, and the energies of the reactants/products were connected with the energies of end points of the calculated reaction coordinates by straight lines.

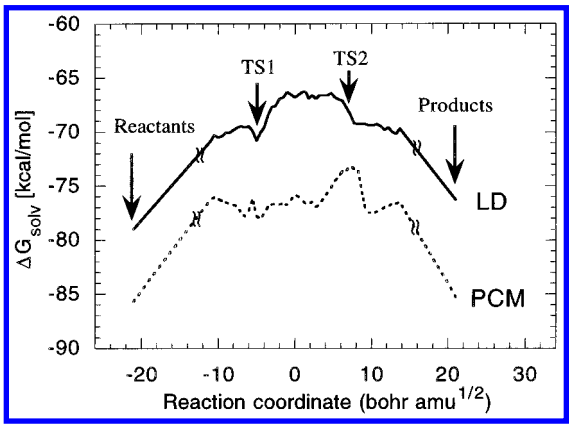

Figure 9. Comparison of the LD and PCM solvation free energies calculated along the reaction coordinate for the associative hydrolysis of methyl phosphate monoanion ($H_2O + MeOPO_3H^- \rightleftharpoons H_2PO_4^- +$ MeOH).

from −0.82*e* in the ground state to −1.02*e* in the transition state for the H_2O attack at $MeOPO_3H^-$ (TS1), whereas charges on the transferred proton and phosphorus remain nearly the same as in the corresponding reactants (Figures 3 and 4). The charge transfer toward the attacking oxygen is counterbalanced by a decrease in charge on the ionic oxygen, which gradually changes into ester oxygen. As the reaction coordinate progresses from TS1 to the pentavalent intermediate $MeOPO_4H_3^-$, the excess charge is transferred from the attacking oxygen to phosphorus and later, in TS2, to the oxygen on the leaving group. From this picture, one can suggest that an optimal catalyst should be capable of stabilizing negative charge on both the leaving and attacking group in the TS2 and TS1 structures. This can be accomplished, for example, by a two-metal ion catalytic mechanism utilized in the exonuclease active site of DNA polymerase I.[57]

The *hydrolysis of neutral methyl phosphoric acid*, $MeOPO_3H_2$ (Figure 3), has mechanistic features similar to the associative

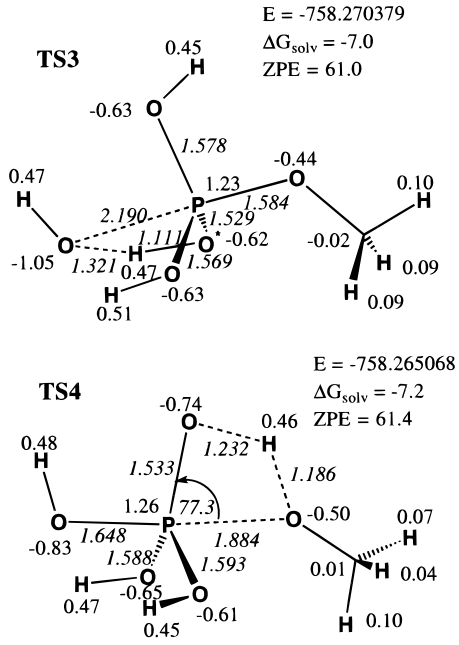

Figure 10. Structures of the transition states for the associative hydrolysis of methyl phosphate. The TSs considered lead to the neutral pentavalent intermediate. For notation see the legend of Figure 3.

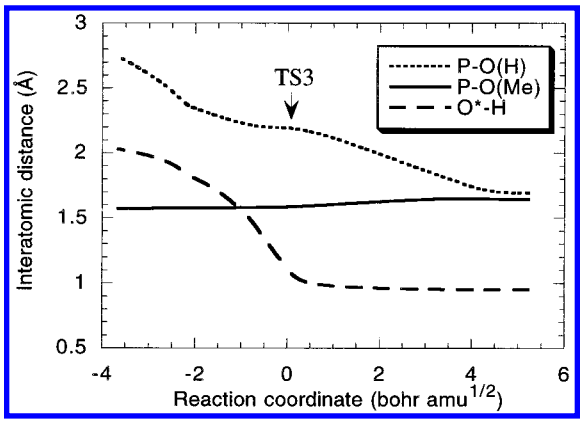

Figure 11. Variation of the axial PO bond lengths and the proton position along the HF/6-31G* intrinsic reaction coordinate proceeding via the TS3 structure (Figure 10).

hydrolysis of the methyl phosphate monoanion, which was discussed in preceding paragraphs. Namely, the reaction coordinate proceeds via two transition states, denoted TS3 and TS4 (Figure 10), which are separated by the neutral pentavalent reaction intermediate, $MeOPO_4H_4$ (Figure 4). Also the geometric differences between the neutral and monoanionic transition structures are subtle and involve for example shorter axial PO bonds and smaller OPO angles between axial and equatorial oxygens in the neutral transition structures. Furthermore, as the additional hydrogen on the neutral substrate is free to rotate, several stable rotational isomers can be expected to exist for TS3 and TS4 transition states. Since such isomerism is expected to give negligible contributions to the energetics of the hydrolysis reaction, we considered only the conformers depicted in Figure 10. Because of a smaller proton affinity of the neutral substrate, the proton-transfer step in the neutral water attack is delayed and contributes about 98% to the total change in the IRC in the TS3 transition state (Figure 11). Analogously, TS4 is dominated by the proton transfer between phosphate and methoxide oxygens. Because the structures with symmetric hydrogen bonds, in which the proton is positioned near the central region, are usually slightly destabilized by solvation, the

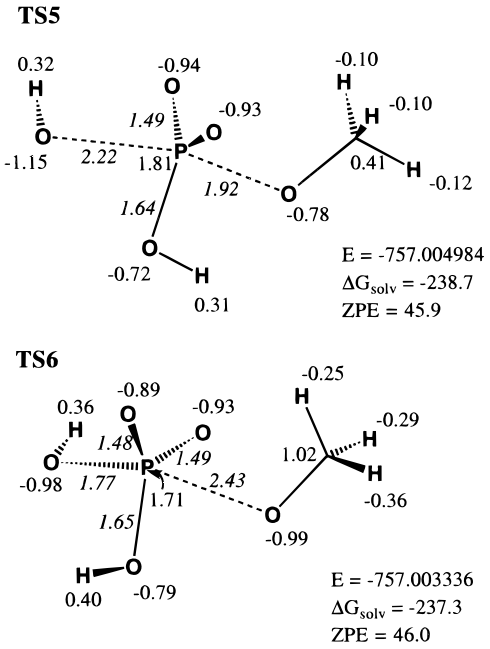

Figure 12. Structures of the dianionic transition states for the associative hydrolysis of methyl phosphate. For notation see the legend of Figure 3.

TS positions on the reaction coordinate are not expected to be shifted by solvation effects.

To obtain a complete mechanistic picture of the hydrolysis of the neutral methyl phosphate (acid-catalyzed hydrolysis), one should also consider the preequilibrium formation of the OH^- + $MeOPO_3H_3^+$ ion pair. Because the pK_a of the methyl phosphate is −3, this step is about 26 kcal/mol uphill (Table 1). This proton-transfer energy is less than the activation barrier for phosphate hydrolysis in low pH (33 kcal/mol). Consequently, the related mechanism of the OH^- attack on the protonated phosphate cannot be excluded. However, this mechanism was not studied by us since (as discussed in the paragraph devoted to the monoanion hydrolysis) the transition states for the H_2O and OH^- attack are expected to have similar structures and energies. Distinguishing unambiguously these TS structures and energies without using analytical derivatives of the solvation energies is a practically impossible task.

The geometric and topological features of the *dianionic associative mechanisms* are markedly different from the neutral and monoanionic case. First, there are two alternative dianionic pathways, and each of them involves only one transition state and no intermediate. These transition states are denoted as TS5 and TS6 (Figure 12). The latter feature resembles mechanistic details of the bimolecular nucleophilic substitution reactions (S_N2) on saturated carbon atoms. The nucleophilic attack and departure of the leaving group are synchronized in such a way that the difference in distances between phosphorus and the axial oxygen atoms, PO(Me) − PO(H), is proportional to the reaction coordinate (Figure 13). Moreover, the distance between two axial oxygens, PO(Me) + PO(H), remains constant in the vicinity of the transition state. Second, the gas-phase and solution geometries of the dianionic transition states are somewhat different (Figure 14). Thus, the geometries presented in Figure 12 correspond to the positions of the highest free energy point along the reaction coordinate in solution. This point was obtained by pointwise corrections of the gas-phase reaction coordinate for both electron-correlation and solvation effects (as shown in Figure 14). Finally, it is the hydroxide and methoxide ion that play the role of the nucleophile and the

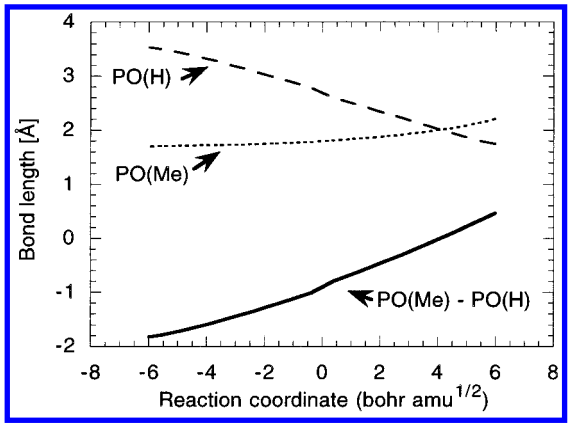

Figure 13. Variation of the axial PO bond lengths along the reaction coordinate passing through the TS6 transition state.

leaving group in the dianionic associative mechanisms involving TS5 and TS6 transition structures. However, as in the case of the monoanionic associative mechanism, the transition states for the attack of the hydroxide ion on the phosphate monoanion and for the attack by neutral water molecule on the phosphate dianion are assumed to have very similar structures and energies. Although computational limitations made it hard to rigorously verify this picture, it is strongly supported by our study of the related case of the neutral water attack on the less basic phosphate monoanion. In other words, because the proton-transfer step precedes the formation of the new PO bond in the neutral water attack on the phosphate monoanion, these events should occur in the same order for the neutral water attack on phosphate dianion, which has larger proton affinity. Consequently, the TS is formed following a full proton transfer between the water oxygen and the phosphate, and the structure of this TS should be nearly identical with that of TS6.

Because the proton that is being transferred to the phosphate remains oriented toward the attacking oxygen, neutral water attack on the phosphate dianion can only proceed via such a TS6-like structure. In contrast, there are two alternative pathways (TS5 and TS6) for the attack by the hydroxide anion on the monomethyl phosphate monoanion. These two hydrolytic pathways differ in the orientation of the phosphate hydrogen with respect to the attacking nucleophile (Figure 12). If the (P)O−H bond points toward the attacking group, the transition state for the substitution reaction is late; that is, the attacking oxygen must come close to the phosphorus atom in the productive trajectory. The critical P−O distance is about 1.8 Å for the attack of the hydroxide ion (TS6) and about 1.9 Å for the reverse reaction (i.e. for the proton-assisted nucleophilic attack of the methoxide ion on the phosphate monoanion (TS5)). Alternatively, the transition state occurs early if the (P)O−H bond points toward the oxygen of the leaving group. In addition to the asymmetric transition states TS5 and TS6 we examined possible transition structures for which the phosphorane hydroxyl lies in the equatorial plane and the axial PO bonds have similar lengths. This search resulted only in a local maximum (saddle point of the second order), which was in solution somewhat less stable than the TS6 structure. However, the corresponding free energy surface in solution was found to be very flat. In fact, because we searched the free energy surface in this region only manually in a limited number of points, and because there is about 1% grid-related uncertainty of our ΔG_{solv} values, we cannot exclude a possible existence of a shallow (∼3 kcal/mol) minimum in this region of the free energy surface.

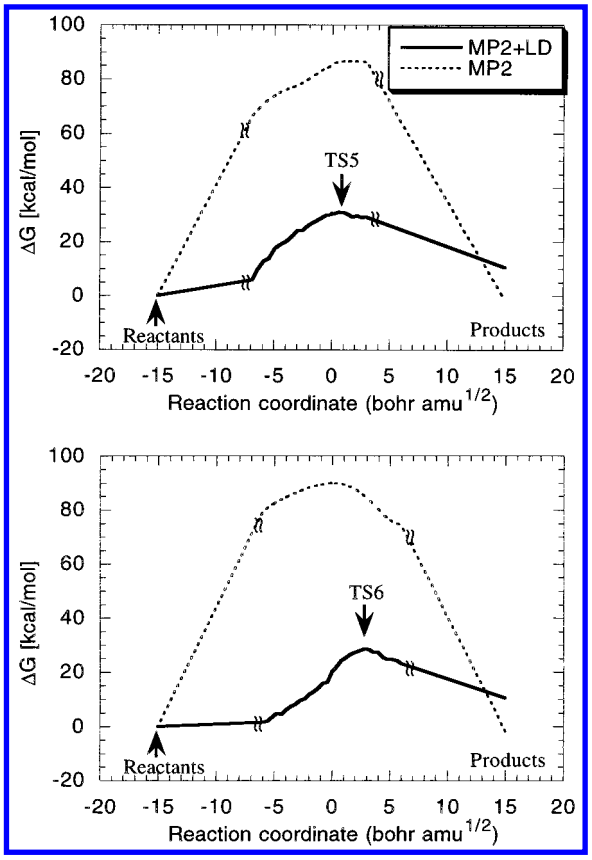

Figure 14. Comparison of the calculated energy and free energy profiles of the $OH^- + MeOPO_3H^- \rightleftharpoons H_2PO_4^- + MeO^-$ reaction in the gas phase (MP2/6-31+G** energy differences, dotted line) and aqueous solution (LD + MP2/6-31+G** free energy differences, solid line). The upper and lower plots correspond to the IRC proceeding via the TS5 and TS6 structure, respectively (Figure 12). Origins (i.e., zero values) of these reaction coordinates correspond to the gas-phase HF/6-31G* geometries of TS5 and TS6. The TS5 IRC calculation (upper plot) was terminated for the reaction coordinate values of −6.9 and 3.0 bohr amu.$^{1/2}$ The distance between phosphorus and the oxygen of the attacking (OH^-) and leaving (MeO^-) group reached 2.51 and 2.75 Å, in these terminal points, respectively. The corresponding terminal points for the TS6 IRC calculation (lower plot) were −6.0 and 6.0 bohr amu$^{1/2}$, or P−O(H) = 3.53 Å and P−O(Me) = 2.21 Å, respectively. The values at which reaction coordinates reach reactant (i.e., infinitely separated OH^- and $MeOPO_3H^-$) and product (i.e., infinitely separated $H_2PO_4^-$ and MeO^-) structures were incidentally chosen to be ±15 bohr amu$^{1/2}$, and the relative MP2 and MP2+LD energies of reactants were set to 0 kcal/mol. The end points of the calculated reaction coordinates were connected with reactants and products by straight lines.

The question whether the dianionic phosphorane represents a reaction intermediate has been intensively pursued by several research groups.[13−16] This question may be important when the intermediate is at much lower energy than its two neighboring TSs. However, when we have an intermediate whose depth is only slightly lower than the surrounding TS, the reaction rate is practically identical with that of the same height. In this case the frequently stated point that the intermediate "does not live a long time" is not so meaningful since the actual lifetime is determined by the height of the given $\Delta g(x)$ and not the exact shape at the top of the barrier. In other words, what counts is the energetics and not the exact form of the surface.

The comparison of the atomic charges in the reactants (OH^- and $MeOPO_3H^-$, Figure 3) and in TS5 shows that the electron density is transferred in TS5 from the hydroxide ion and phosphorus to the equatorial ionic oxygens and to the oxygen of the leaving group. A similar behavior is observed in TS6

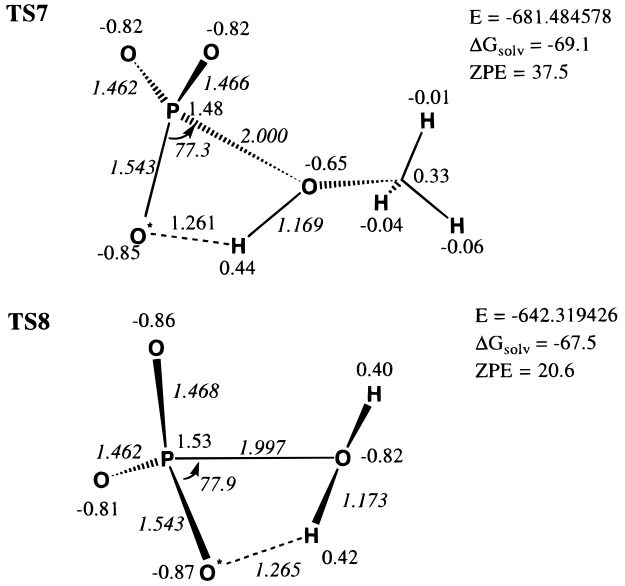

Figure 15. Structures of the transition states for the dissociative hydrolysis of the methyl phosphate monoanion. For notation see the legend of Figure 3.

when its charge density is compared to OH^- and $MeOPO_3H^-$. On the other hand, when the charge distribution of TS6 is compared to H_2O and $MeOPO_3^{2-}$, it is found that the negative charge density increases on the attacking oxygen and decreases on the equatorial oxygens. However, the latter comparison is less relevant because the proton transfer from H_2O, which occurs before the transition state is reached, results in a significant charge redistribution on the nucleophile and substrate.

3.2.2. Dissociative Mechanisms. The structures of the transition states for the *dissociation of the monomethyl phosphate monoanion* into PO_3^- and methanol (TS7) and for the subsequent attack on metaphosphate by H_2O (TS8) are shown in Figure 15. The calculated IRC values for these TSs are dominated by the proton transfer between the phosphate oxygen and the leaving or attacking group (Figure 16). However, the position of TS7 and TS8 slightly shifts (by about 0.5 bohr amu$^{1/2}$) toward the product state (Figure 17) upon taking into account electron correlation and solvation effects. A closer inspection of the IRC for the solvated TS7 and TS8 (Figure 16) shows that the proton is nearly transferred to the axial oxygen (the corresponding O*−H and O−H distances are about 1.5 and 1.05 Å) and that the P−O(H) and P−O(Me) distances become slightly longer than in the gas-phase structures. The solvation effect was found to be more pronounced for TS8. This quantitative difference in solvation of TS7 and TS8 originates from the large difference in the solvation free energies of the OH^- and CH_3O^- ions.[32] Apparently, more solvation is lost upon transfer of a proton from phosphate to the OH^- nucleophile (TS8) than upon transfer to CH_3O^- (TS7).

The free energy profile or more exactly the PMF along the dissociative pathway for the hydrolysis of the methyl phosphate anion (Figure 17) is similar to the profile of the associative hydrolysis (Figure 8) in that it involves two transition states and a reaction intermediate. Apparently the proton transfer contributes significantly to the reaction coordinate in the TS7 and TS8 transition states and the corresponding activation barriers are more narrow than the barriers calculated for the associative reaction. Thus one can expect substantial positive kinetic isotope effects to be observed for the dissociative hydrolysis of methyl phosphate monoanion. Both associative and dissociative reactions are slowed down by aqueous solva-

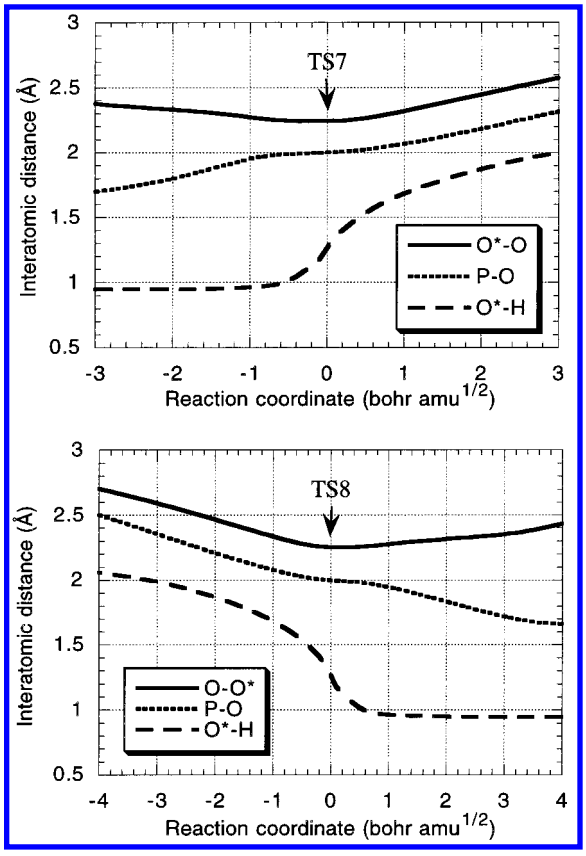

Figure 16. Variation of the interatomic distances along the reaction coordinate for the dissociation of the methyl phosphate monoanion into PO_3^- and MeOH (top) and for the nucleophilic attack of H_2O at the phosphorus atom of PO_3^- (bottom). The transition-state structures (TS7, TS8) correspond to the zero values of the reaction coordinates. O denotes the oxygen atom in MeOH (top) or H_2O (bottom) nucleophiles, and O* denotes the anionic oxygen that exchanges a proton with O during the course of the reaction (Figure 15).

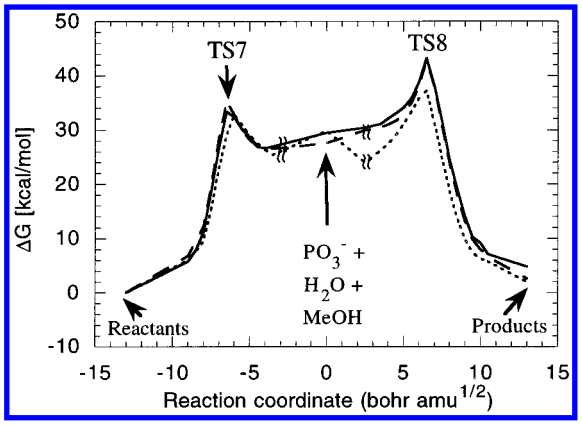

Figure 17. Calculated energy and free energy profiles of the reaction $MeOPO_3H^- + H_2O \rightleftharpoons PO_3^- + MeOH + H_2O \rightleftharpoons H_2PO_4^- + MeOH$ in the gas phase (MP2/6-31+G** energy differences, dotted line) and aqueous solution (LD + MP2/6-31+G** free energy differences, solid line; PCM + MP2/6-31+G** free energy differences, dashed line). The reaction coordinate was composed from the two independent IRC runs started from TS7 and TS8 structures, the infinitely separated reactants, products, and "intermediate" PO_3^-, MeOH, and H_2O molecules. The values of the reaction coordinate for the reactants, TS7, intermediate, TS8, and products were chosen arbitrarily as −13, −7, 0, 7, and 13 bohr amu$^{1/2}$, respectively. The end points of the calculated reaction coordinates were connected with reactants, products, and intermediates by the straight lines.

tion, although solvation effects are slightly more pronounced in the associative case. Interestingly, our calculations show that

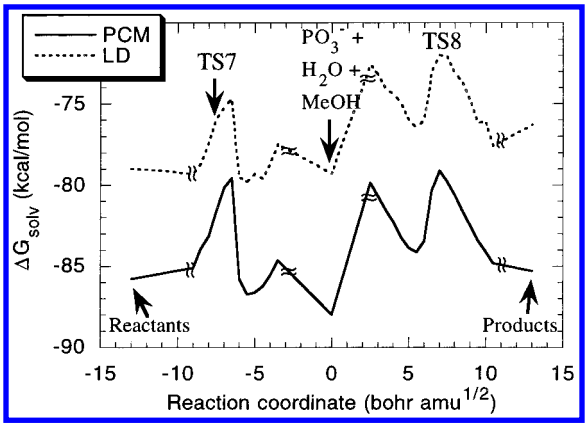

Figure 18. Solvation free energy (ΔG_{solv}) as a function of the reaction coordinate for the dissociative hydrolysis of methyl phosphate anion. For details about the construction of the reaction coordinate see the legend of Figure 17.

the kinetic barrier for the dissociative hydrolysis does not correspond to the dissociation of methyl phosphate anion (TS7), but to water attack on the metaphosphate ion (TS8). This is mainly due to solvation destabilization of TS8 by the surrounding solvent, which was obtained by both LD and PCM solvation models (Figure 18). The dissociative mechanism that does not involve a proton transfer from phosphate to the leaving group ($MeOPO_3H^- \rightleftharpoons PO_3H + MeO^-$) can be excluded, on the basis of the corresponding energy value (Table 1). Thus, we did not explore this reaction coordinate in the present study.

The formation of unstable metaphosphoric acid, PO_3H, is more probable in acidic solution via the *dissociation of the neutral methyl phosphate* ($MeOPO_3H_2 \rightleftharpoons PO_3H + MeOH$). In the corresponding gas-phase transition state structure (TS9), the proton is halfway transferred to the oxygen of the leaving group, but the P−O(Me) bond is very short (1.76 Å). A very similar gas-phase structure was found for the transition state for the subsequent attack of H_2O on PO_3H (TS10). Because the energies of these TSs are well above those of the associative hydrolysis of the neutral methyl phosphate and also because the corresponding acid-catalyzed reactions are of less importance in biochemistry, we do not provide here the detailed geometric structures nor the MP2 and solvation corrections along the corresponding reaction coordinates.

The *dissociative hydrolysis of methyl phosphate dianion* is facilitated in the gas-phase by repulsive electrostatic forces between ions that carry the same charge. As a result, the gas-phase energy of the infinitely separated metaphosphate and methoxide ions is about 40 kcal/mol lower than the energy of the methyl phosphate dianion (Table 1, Figure 19). This relative energy is reversed in aqueous solution because the solvation energy of the dianion is approximately 80 kcal/mol larger (in absolute value) than the sum of solvation energies of PO_3^- and MeO^- (for calculated solvation energies see Figures 3−5). The barrier for the dissociative hydrolysis of methyl phosphate dianion corresponds to the metaphosphate ion or to its weakly associated complex with the leaving and/or attacking ions since the calculated MP2+LD free energy stays almost constant for PO distances > 3.3 Å (Figure 19).

4. Free Energy Surfaces for Phosphate Hydrolysis

The analysis of competing mechanisms has been a primary objective of physical organic chemists for a long time.[58] Significant progress has been made in classifying reactions using

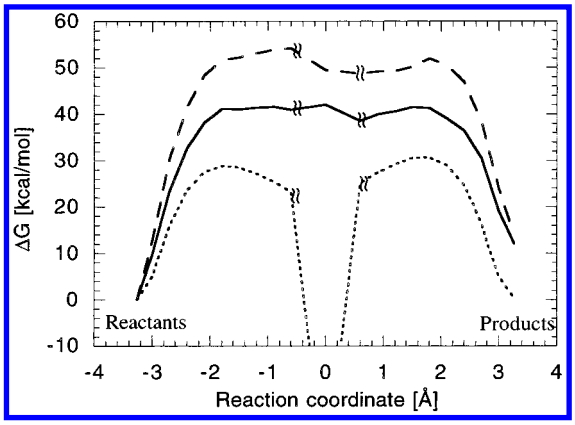

Figure 19. Calculated energy and free energy profiles of the reaction $MeOPO_3H_2$- + $OH^- \leftrightarrows PO_3^-$ + MeO^- + $OH^- \leftrightarrows HPO_4^{2-}$ + MeO^- in the gas phase (MP2/6-31+G** energy differences, dotted line) and aqueous solution (LD + MP2/6-31+G** free energy differences, solid line; PCM + MP2/6-31+G** free energy differences, dashed line). The reaction coordinate (RC) was associated with the distance between phosphorus and oxygen of the leaving or incoming group using the relationship RC = PO(Me) − PO(H), where the PO distance of 5 Å was used for the infinitely separated ions. For example, the reaction coordinate corresponding to the PO(Me) bond length of 3 Å amounts to 3 − 5 = −2 Å. The reaction coordinate was varied in increments of 0.1 Å, while other degrees of freedom were fully optimized at the HF/6-31G* level. These relaxed potential energy scans were initiated at the geometry of the reactants and products and terminated for PO distances of 4.4 Å (RC = ±0.6 Å). The relative energy (including the ΔZPE contribution) of infinitely separated PO_3^-, MeO^-, and OH^- (RC = 0 Å) was connected with the end points of the relaxed potential energy calculations by the straight lines.

diagrams of the type introduced by More O′Ferrall[59] and Jencks.[60] These diagrams can be considered as variants of the *potential energy* surfaces introduced by Eyring and Polanyi[61] except that More O′Ferrall and Jencks considered *free energies* and used the corners of their diagrams to describe the asymptotic states (i.e., reactants, products, and reaction intermediates). In the absence of direct information about the transition-state structure it was assumed that its properties are proportional to the corresponding linear free energy relationship (LFER) parameters.[60] Although such diagrams offered a powerful link between experimental and theoretical views of organic reactivities, they could not provide a quantitative description of reactivity due to the lack of prescriptions for estimating the free energy along the reaction coordinates. Attempts to quantify the More O′Ferrall−Jencks (MOFJ) diagrams by drawing gas-phase potential energies as functions of *bond orders* were reported,[62] but these studies are less relevant to chemistry in solution. *Quantitative* studies that provided two-dimensional free energy surfaces for chemical reactions in solution were first reported by Warshel and co-workers (see, for example, refs 45, 63), who used the EVB approach to guarantee that the energies at the corners of the surface reproduce the experimental free energies for solution reactions. These EVB studies indicated that in solution one can use *interatomic distances* as reasonable coordinates for the MOFJ type free energy diagrams since the PMF at relatively small interaction distances is similar to that at infinite separation (see eq 7). In contrast, the gas-phase reactants can interact even at large distances, and for the construction of MOFJ diagrams the interatomic distances or bond lengths need to be replaced by bond orders[62] or other parameters.

This work tries to provide the first step toward the construction of general free energy surfaces for phosphate hydrolysis in solution and proteins. In constructing such surfaces, we are restricted by the requirement to reserve the *z* axis for the value of the relevant free energy. This confines us to two-dimensional reaction coordinates. Thus, we are forced to focus on the dependence of the free energy on the P−O(H) and P−O(Me) distances (which are taken as the *x* and *y* axes, respectively) and minimize the free energy with regards to all other coordinates, including of course the solvent. However, since the phosphate monoesters are polyprotic acids, information about the proton position is essential for the detailed understanding of the mechanism of its hydrolysis, and as such it cannot be fully neglected in the free energy diagrams. Therefore, we have tried to provide at least a minimal amount of data about the proton configuration. First, we indicate the possible equilibrium proton positions in the form of the type of the attacking nucleophile (H_2O versus OH^-) and consider the reaction coordinates that involve these asymptotic states (see Figures 20 and 21). Second, we provide here some information about the energetics of the proton-transfer process by using dashed lines on the side of the main free energy diagrams (Figures 20−22). Naturally, this leads to rather complex diagrams whose fine details should only be examined by those who are interested in such details. The overall picture can be considered only in terms of the heavy atom coordinates. Note, however, that the calculated activation barriers for heavy atom transfer reflect the contributions associated with the corresponding proton-transfer processes. Thus, for example, the energetics of TS7 involves the barrier for transferring the proton from the phosphate oxygen to the leaving group.

Our two-dimensional free energy diagrams and the character of stationary points can be used for a unique *classification of reaction mechanisms*. Such a quantification is needed to clarify and simplify vague qualitative statements as “an associative mechanism with a dissociative transition state” or “ a dissociative mechanism with some associative character” that appear in the literature. In fact, the need for the unambiguous characterization of the reaction mechanisms acting in phosphate ester hydrolysis reactions has recently been pointed out by Mildvan,[64] who proposed classification based on the bond order to the axially entering group. However, the relationship used by Mildvan to relate the PO bond orders with the bond lengths observed in crystal structures was originally proposed for bonding in metals.[65] When this equation is applied to the PO bonds, zero bond orders are obtained for the PO bond lengths larger that 2.5 Å. This distance is much smaller than the sum of the van der Waals radii of P and O atoms (3.3 Å),[41] which means that the bond order values decrease unreasonably fast with the PO distance. As a result, this classification scheme overestimates the dissociative character of the PO bond cleavage reactions in enzymes.

Here we denote reaction pathways that lie above and below the diagonal line connecting the reactant and product corners of the free energy diagram as associative and dissociative, respectively. In addition, mechanisms involving a transition-state barrier and no intermediate along their path will be described as concerted. Concerted mechanisms may have either associative or dissociative character, which is determined according to the previous rule. According to the suggestion of Cox and Ramsay,[1] the S_N2 and S_N1 classification system is avoided since these terms have been loosely used in the literature in such a way that many readers infer from them mechanistic details that are true only for the S_N2 and S_N1 reactions at saturated carbon atoms.

Our calculated free energy surfaces (Figures 20−22) represent the energetics of the given reaction in terms of the corresponding

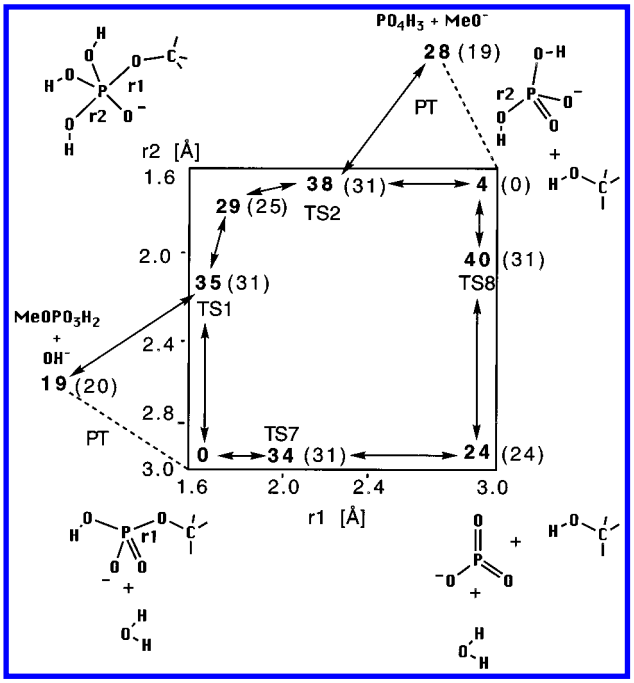

Figure 20. MP2 + LD free energy surface for the hydrolysis of monomethyl phosphate monoanion. The calculated relative free energies (kcal/mol, boldface) are presented as a function of the bond length between phosphorus and oxygens of the incoming (r2) and leaving (r1) groups. Our best free energies estimates based on a critical consideration of both the calculated and experimental data are given in parentheses. The corners of this diagram are occupied by the reactants (lower left corner), products (upper right corner), and the pentacovalent and metaphosphate intermediates. Reaction mechanisms and transition states discussed in the text are indicated by arrows and "TS", respectively. The presence of two different mechanisms reaching some transition states indicates that an additional TSs is present in this (r1, r2) region and that these TS are numerically indistinguishable. The dashed lines indicate proton-transfer (PT) steps.

potential of mean force (PMF). The construction of these surfaces and the treatment of concentration effects is discussed in section 2.3.

4.1 Experimenal Considerations. Before proceeding to the analysis of the calculated results it is useful to keep in mind the relevant experimental background. Experimental studies of the hydrolysis of phosphate monoesters in aqueous solution[66−68] have established a characteristic pH dependence of the reaction rate, in which the maximum rate occurs at about pH 4−5. In more alkaline solution the rate steadily decreases, while in more acidic media a minimum rate is reached around pH 1 (1 M H_3O^+) and increases again at lower pH. More specifically, the first-order rate constant decreases from 8×10^{-6} s^{-1} at pH 4 to 3.5×10^{-6} s^{-1} at pH 1, and to 1.3×10^{-6} s^{-1} at pH 7.5 for monomethyl phosphate hydrolysis measured at 100 °C.[68] For more alkaline solutions, the reaction rate falls below the detection limits. Consequently, an *upper limit* for the rate constant of hydrolysis of methyl phosphate *dianion* was set at 5×10^{-8} s^{-1}.[68] Because of considerable reaction rate differences between the pH regions in which the neutral (pH ∼ 1.6), monoanionic (pH ∼ 4), and dianionic (pH ∼ 7) forms of methyl phosphate predominate, it seemed to be clear[1,66−68] that the monoanion can exploit a special reaction mechanism that supersedes all other mechanisms. This mechanism was proposed to involve a dissociative reaction pathway with the monomeric metaphosphate intermediate (PO_3^-).[66−68]

4.2. Methyl Phosphate Monoanion. The free energy diagram for the hydrolysis of the methyl phosphate monoanion is shown in Figure 20. Pathways along or in the vicinity of the top-left and lower-right corners can clearly be characterized as pure associative and dissociative mechanisms, respectively. The free energy surface in the central part of this diagram was not studied in this work, but our study of the methanolysis of the methyl phosphate monoanion[69] indicates that there is no concerted low-energy pathway going through this region of the diagram. The comparison of the calculated activation barriers ($\Delta G^{\ddagger}$) for the associative and dissociative mechanism shows that the dissociative mechanism is not preferred to the associative one. In fact, our results indicate that the associative hydrolysis of the methyl phosphate monoanion should be about 10 times faster (at 298 K). However, this result should be considered with caution because the corresponding $\Delta\Delta G^{\ddagger}$ of 1.4 kcal/mol is smaller than the error bar of our computational method and the approximation used in eq 6. Nevertheless, because of considerable structural similarity of TS2 and TS8 transition states, systematic computational errors can be expected to partially cancel out for the $\Delta\Delta G^{\ddagger}$ difference between the rate-limiting steps in associative and dissociative mechanisms. Further support for the preferred associative pathway is provided by the comparison of the calculated kinetic isotope effects (Table 3) with the experimental solvent isotope effects (kH_2O/kD_2O) of 0.87 and 0.99 measured for methyl phosphate hydrolysis at pH 4 and 4 M $HClO_4$, respectively.[68]

As we indicated in section 3.2.1, the activation barriers for the H_2O attack on the methyl phosphate monoanion and for OH^- attack on $MeOPO_3H_2$ cannot be distinguished by the present calculations. This might be viewed by some as a drawback of our computational methodology. However, it is important to note that these two mechanisms are also indistinguishable by kinetic experiments.[68,70] This point is quite important in view of the unjustified assumptions made in previous studies of this reaction. That is, the possibility that the hydrolysis of phosphate monoanion by H_2O can go through $OH^- + MeOPO_3H_2$ was rejected by Vernon and co-workers[68,71] on the basis of the assumption that the energetics of the OH^- attack on $MeOPO_3H_2$ is identical with that of the attack of OH^- on trimethyl phosphate. This assumption has been generally accepted.[1,72] Since the arguments of Vernon et al. involve free energy differences as large as 12 kcal/mol, we were able to credibly demonstrate that Vernon's estimate of the energetics of an OH^- attack on the neutral methyl phosphate was not justified.[4] Consequently, the above-mentioned reaction mechanisms share a common transition state structure (TS1) in Figure 20. This does not represent a violation of the rule that a first-order saddle point can have only one transition vector,[73] but merely the numerical coincidence. In reality, the activation free energies for the H_2O attack at the methyl phosphate monoanion and for the OH^- attack on $MeOPO_3H_2$ may slightly (±2 kcal/mol) differ so that the OH^- attack on $MeOPO_3H_2$ may be slightly faster or vice versa. The OH^- attack on $MeOPO_3H_2$ might be favored, for example, by the nonequilibrium solvation effects (solvent reorganization) since no major charge redistribution occurs during this reaction.

The calculated activation barrier of 38.3 kcal/mol for the rate-determining step of this reaction is larger by 7 kcal/mol than the barrier derived from the measured rate of hydrolysis by using eq 2. This overestimation is similar to that for the products (upper-right corner), and it probably originates from the additive effects of small systematic errors involving both the gas-phase and solvation energetics (see also section 5). The calculated barrier corresponding to the TS1 transition state (34.5 kcal/mol) is in better agreement with the experimentally determined activation energy of 31 kcal/mol, since TS1 is structurally closer

TABLE 3: Calculated Activation Free Energies and the Kinetic Isotope Effects for the Monomethyl Phosphate Hydrolysis Reactions

reactants	TS	$\Delta E_{MP2}^{\ddagger}$	$\Delta ZPE^{\ddagger}$	$\Delta G_{LD}^{\ddagger}$	$\Delta G_{PCM}^{\ddagger}$	$T\Delta S'_{tr}{}^{a}$	$T\Delta S'^{b}$	$\Delta g^{\ddagger c}$	$\Delta G^{\ddagger d}$	$k_H/k_D{}^{e}$
				Associative Pathways						
$MeOPO_3H^- + H_2O$	TS1	23.8	1.0	8.3	7.8	−5.5	−6.8	33.1	34.5	0.9
	TS2	24.6	1.1	11.2	12.7	−5.5	−6.3	36.9	38.3	0.6
$MeOPO_3H_2 + H_2O$	TS3	19.1	0.9	11.2	9.0	−5.5	−7.5	31.2	32.6	1.3
	TS4	22.4	1.3	10.8	8.2	−5.5	−8.1	33.5	34.9	1.1
$MeOPO_3^{2-} + H_2O$	TS5	22.1	0.5	16.2	17.3	−5.5	−5.1	38.8	40.2	0.9
	TS6	23.1	0.6	17.6	22.3	−5.5	−5.8	41.3	42.7	0.6
				Dissociative Pathways						
$MeOPO_3H^-$	TS7	34.0	−2.8	2.4	3.9	0.0	−0.1	33.6	33.6	2.3
$MeOPO_3H^- + H_2O$	TS8 + MeOH	37.2	−1.5	5.1	5.3	0.3	0.6	40.8	39.8	1.5
$MeOPO_3H^{2-}$	$MeO^- + PO_3^-$	−37.3	−3.6	82.8	90.6	5.7	5.3	41.9	39.5	1.0
$MeOPO_3H_2$	TS9	39.9	−1.8	−1.4	−0.7	0.0	−1.0	36.7	36.7	2.7
$MeOPO_3H_2 + H_2O$	TS10 + MeOH	46.6	−1.0	−1.3	0.2	0.3	−0.4	44.3	43.3	1.3

[a] $\Delta S'_{tr}$ denotes the change in translational entropy during the reaction, evaluated for 1 M ideal gas and scaled by 2/3 (see section 2.3). The temperature is taken as $T = 298$ K. [b] $\Delta S'$ is taken as the sum of $\Delta S'_{tr}$, and the change in rotational and vibrational entropy during the reaction for 1 M ideal gas. [c] $\Delta g^{\ddagger} = \Delta E_{MP2}^{\ddagger} + \Delta ZPE^{\ddagger} + \Delta G_{LD}^{\ddagger} - \alpha T\Delta S'$ (kcal/mol), where individual contributions (see legend to Table 1 for their notation) were obtained as the difference between the energies of TS and the sum of energies of the infinitely separated reactants. [d] Activation free energy for standard state of 1 M aqueous solution and 55 M H_2O (see section 2.3). [e] The ratio of the reaction rates for the standard and the O-deuterated substrate and nucleophile (k_H/k_D) at 100 °C. k_H/k_D was estimated from the difference in zero-point vibrational energies ($\Delta ZPE^{\ddagger}$): $k_H/k_D = \exp[(\Delta ZPE_D^{\ddagger} - \Delta ZPE_H^{\ddagger})/kT]$.

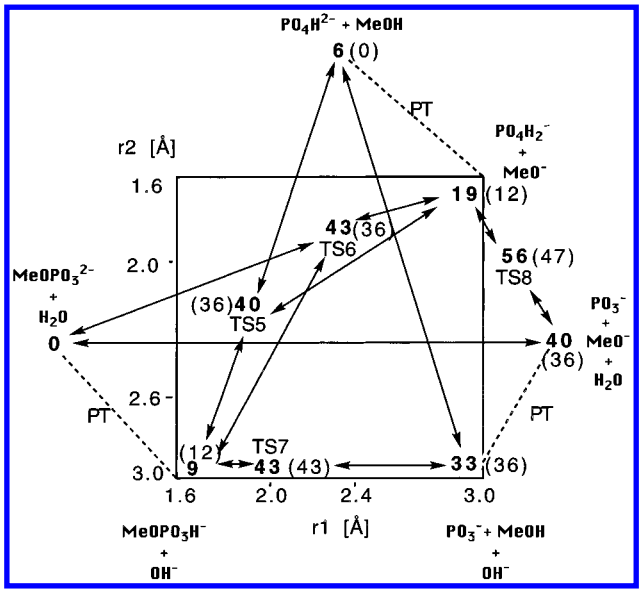

Figure 21. MP2+LD free energy surface (kcal/mol) for the hydrolysis of monomethyl phosphate dianion. The notation used in this plot is identical with that presented in Table 3 and the legend of Figure 20.

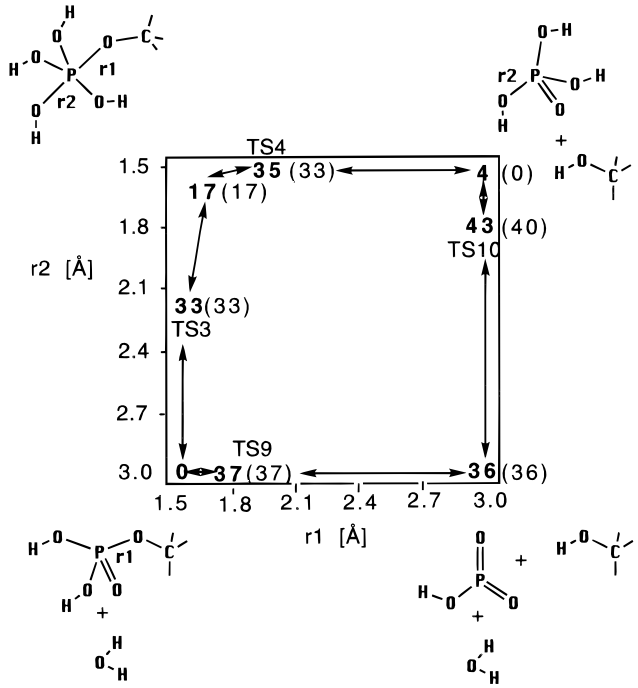

Figure 22. MP2+LD free energy surface (kcal/mol) for the hydrolysis of neutral monomethyl phosphate. The notation used in this plot is identical with that presented in Table 3 and the legend of Figure 20.

to the reactants and its energy is less affected by the systematic overestimation of the productlike structures. A similar trend was calculated also for the TS7 and TS8 barriers. In contrast, the experimental observation that methyl phosphate hydrolysis in $H_2{}^{18}O$ does not yield an ^{18}O-containing substrate[68] indicates that the activation energy for the OH^- or H_2O attack (TS1) should be equal or larger than for the elimination of methanol or methoxide ion (TS2). Similar reasoning applies also for the relative heights of the TS7 and TS8 barriers, provided that the reaction proceeds via the dissociative mechanism.

For the sake of future analysis, we list in Table 3 contributions to the activation barriers in aqueous solution. In addition, the values of relative free energies that were extrapolated from the experimental and our calculated results are given in parentheses in Figures 20−22. These data can be considered as the best estimates available for the free energy surface of the methyl phosphate hydrolysis.

4.3 Methyl Phosphate Dianion. A hydrolytic reaction that starts from the methyl phosphate dianion (Figure 21) can proceed to the $PO_3^- + MeO^- + H_2O$ state via a monotonically uphill *dissociative mechanism* and from there via another barrierless transition to the product valley. The calculated activation energy for this mechanism is 40 kcal/mol. This barrier is identical with the barrier for the dissociative hydrolysis of the monoanion (Figure 20), whereas experimentally methyl phosphate monoanion was found to be at least 100 times more reactive than the dianion.[68] The second part of the dissociative hydrolysis of the methyl phosphate dianion was predicted to involve the OH^- attack on PO_3^-, and not the attack by neutral water. An alternative dissociative mechanism, which is initiated from the preequilibrium $MeOPO_3H^- + OH^-$ structure, is practically identical with the mechanism discussed in section 4.1. Here, however, an additional 12 kcal/mol is required for

the initial proton-transfer step, so that this mechanism has a total activation barrier of 43 kcal/mol and can be probably excluded.

The dissociative pathway can be bypassed via three different *concerted pathways* that have *associative* character and similar activation energies (Figure 21). Here the rate-limiting step has an activation energy of 40 kcal/mol, which is 2 kcal/mol larger than the highest calculated barrier for the associative hydrolysis of the monoanion. A better agreement with experimental findings, of at least a 3 kcal/mol difference between the barriers for the dianion and monoanion, can be obtained if one compares the activation barriers for structurally related transition states, i.e., for TS1 and TS5, or TS2 and TS6 (Figures 20 and 21).

As in the case of the monoanion hydrolysis, the calculated activation barriers for the associative and dissociative hydrolysis of the methyl phosphate dianion are very similar (40.2 versus 39.5 kcal/mol, respectively). Taking into account the available experimental data and the systematic overestimation of the productlike structures by our calculations, we obtained consensus activation barriers, which are given in parentheses in Figure 21.

4.4 Neutral Methyl Phosphate. The activation barrier for the associative hydrolysis of the neutral methyl phosphate was calculated to be lower by 8 kcal/mol than for the corresponding dissociative mechanism (Table 3, Figure 22). Thus, it is very unlikely that the dissociative mechanism is involved in the hydrolysis of the neutral methyl phosphate. In contrast to the observed decrease of the reaction rate near pH = 1 (where the neutral methyl phosphate is the dominant species), the calculated rate of the associative hydrolysis of the neutral methyl phosphate is about 100 times faster than for the hydrolytic reaction of the monoanion (Figure 22). However, the slower rate of hydrolysis of methyl phosphate in acidic solution would be consistent with an associative mechanism if nonequilibrium solvation effects were taken into account. That is, while the LD and PCM models involve fully relaxed solvent for each solute configuration, a more rigorous treatment should consider the fact that the transition state in the complete solvent−solute surface involves a maximum with regards to the solvent coordinate (see, for example, 44, 46) rather than a minimum corresponding to the fully relaxed solvent. The magnitude of this effect is related to the magnitude of the so-called "solvent reorganization energy" and is expected to be larger in reactions that involve a large charge separation. The associative hydrolysis of the neutral methyl phosphate belongs to this class of reactions as the proton is transferred in the transition state for this reaction from the attacking water to the neutral phosphate (this results in the temporary formation of an ion pair). Although these issues are of great general importance, their study exceeds the scope of the present paper. Moreover, neutral forms of phosphate monoesters, diesters, and anhydrates are present in very low concentrations under physiological conditions, and therefore the corresponding hydrolytic mechanisms are of lesser biological importance.

5. Concluding Remarks

Understanding the nature of phosphate hydrolysis in biological molecules is of major importance in view of the role of such reactions in many key biological processes. In this paper, we presented the first systematic study of the free energy surfaces for the hydrolysis of methyl phosphate in aqueous solution. We considered the entire range of the substrate protonation states (neutral, monoanion, and dianion) and two forms of the nucleophile that correspond to the hydrolysis by neutral water and by the OH^- ion. The hydrolysis of the neutral methyl phosphate was predicted to proceed via the associative mechanism. For the hydrolysis of the mono- and dianionic methyl phosphates, the associative and dissociative reaction pathways were found to have similar activation barriers. The difference between these barriers is below the error range of our computational methodology (this uncertainty is approximately 4 kcal/mol for structurally similar transition states).

As stated in section 2.2, we evaluated free energy surfaces for the solution reaction using a manual minimization rather than a fully analytical treatment. This approach should not lead to significant errors since the largest solvent effects are associated with changes along the reaction coordinate (leading to the largest changes in the charge distribution) and these changes were mapped systematically by our treatment. More serious errors may be associated with entropic and the first solvation shell effects. The latter include charge transfer to the solvent molecules and the active participation of a bridging water molecule in proton-transfer processes. These effects will be explored in subsequent studies.

Since the present analysis takes into account experimental energy estimates, it provides "consensus" free energy surfaces that can be used in future analyses of different experimental results. In particular, the linear free energy relationships (LFER) have been one of the primary tools in assessing the nature of phosphate hydrolysis in solution (see, for example, ref 74). However, it seems to us that the complex free energy surfaces revealed by the present analysis do not lend themselves to a unique interpretation by LFER without more complete valence bond analysis. That is, both the associative and dissociative paths involve several transition states and proton displacements that must be described by multiple resonance structures (see, for example, refs 9, 57), and the corresponding LFER are therefore not so obvious. For example, our preliminary study indicated that the associative mechanism might not be as sensitive to the nature of the nucleophile as previously thought. Thus, we believe that a combination of experimentally determined trends and theoretical studies should help in advancing the detailed understanding of phosphate hydrolysis.

Finally, it is useful to comment on the biological implication of the present work. Since we find here that the energetics of the associative and dissociative mechanisms in solution are not so different, we conclude that active sites of enzymes could select either mechanism depending on the particular electrostatic environment. Consequently, both mechanisms should be considered in a careful analysis. This conclusion appears to contradict assumptions of some previous mechanistic studies of phosphoryl transfer reactions.[75]

Acknowledgment. This work was supported by the Tobacco Research Grant 4RT-0002. We thank Dr. Jörg Bentzien for reading the manuscript and helpful suggestions.

References and Notes

(1) Cox, J. R., Jr.; Ramsay, O. B. *Chem. Rev. (Washington, D.C.)* **1964**, *64*, 317.

(2) Thatcher, G. R. J.; Kluger, R. *Adv. Phys. Org. Chem.* **1989**, *25*, 99.

(3) Although the classification of mechanisms as associative or dissociative may partially depend on the definition used (see section 3.3), we clearly can talk about two limiting cases where the nature of the transition state is fundamentally different.

(4) Florián, J.; Warshel, A. *J. Am. Chem. Soc.* **1997**, *119*, 5473.

(5) Buchwald, S. L.; Friedman, J. M.; Knowles, J. R. *J. Am. Chem. Soc.* **1984**, *106*, 4911.

(6) Freeman, S.; Friedman, J. M.; Knowles, J. R. *J. Am. Chem. Soc.* **1987**, *109*, 3166.
(7) Friedman, J. M.; Knowles, J. R. *J. Am. Chem. Soc.* **1985**, *107*, 6126.
(8) Frey, P. A. *Tetrahedron* **1982**, *38*, 1541.
(9) Schweins, T.; Warshel, A. *Biochemistry* **1996**, *35*, 14232.
(10) Gorenstein, D. G.; Findlay, J. B.; Luxon, B. A.; Kar, D. *J. Am. Chem. Soc.* **1977**, *99*, 3473.
(11) Gorenstein, D. G.; Luxon, B. A.; Findlay, J. B. *J. Am. Chem. Soc.* **1979**, *101*, 5869.
(12) Hayes, D. M.; Kenyon, G. L.; Kollman, P. A. *J. Am. Chem. Soc.* **1978**, *100*, 4331.
(13) Lim, C.; Karplus, M. *J. Am. Chem. Soc.* **1990**, *112*, 5872.
(14) Uchimaru, T.; Tanabe, K.; Nishikawa, S.; Taira, K. *J. Am. Chem. Soc.* **1991**, *113*, 4351.
(15) Dejaegere, A.; Lim, C.; Karplus, M. *J. Am. Chem. Soc.* **1991**, *113*, 4353.
(16) Yliniemela, A.; Uchimaru, T.; Tanabe, K.; Taira, K. *J. Am. Chem. Soc.* **1993**, *115*, 3032.
(17) Wladkowski, B. D.; Krauss, M.; Stevens, W. J. *J. Phys. Chem.* **1995**, *99*, 6273.
(18) Dejaegere, A.; Karplus, M. *J. Am. Chem. Soc.* **1993**, *115*, 5316.
(19) Dejaegere, A.; Liang, X.; Karplus, M. *J. Chem. Soc., Faraday Trans.* **1994**, *90*, 1763.
(20) Ma, B.; Xie, Y.; Shen, M.; Schleyer, P. v. R.; Schaefer, H. F., III. *J. Am. Chem. Soc.* **1993**, *115*, 11169.
(21) Warshel, A.; Levitt, M. *J. Mol. Biol.* **1976**, *103*, 227.
(22) Warshel, A. *J. Phys. Chem.* **1979**, *83*, 1640.
(23) Tomasi, J.; Persico, M. *Chem. Rev. (Washington, D.C.)* **1994**, *94*, 2027.
(24) Cramer, C. J.; Truhlar, D. G. In *Reviews in Computational Chemistry*; Lipkowitz, K. B., Boyd, D. B., Ed.; VCH: New York, 1993; Vol. 6, p 1.
(25) Chambers, C. C.; Hawkins, G. D.; Cramer, C. J.; Truhlar, D. G. *J. Phys. Chem.* **1996**, *100*, 16385.
(26) Jorgensen, W. L.; Ravimohan, C. *J. Chem. Phys.* **1985**, *83*, 3050.
(27) Field, M. J.; Bash, P. A.; Karplus, M. *J. Comput. Chem.* **1990**, *11*, 700.
(28) Singh, U. C.; Kollman, P. A. *J. Comput. Chem.* **1987**, *7*, 718.
(29) Gao, J. L. *J. Phys. Chem.* **1992**, *96*, 537.
(30) Gao, J. In *Reviews in Computational Chemistry*; Lipkowitz, K. B., Boyd, D. B., Ed.; VCH: New York, 1995; Vol. 7, p 119.
(31) Stavrev, K. S.; Tamm, T.; Zerner, M. C. *Int. J. Quantum Chem.: Quantum Chem. Symp.* **1996**, *30*, 373.
(32) Florián, J.; Warshel, A. *J. Phys. Chem. B* **1997**, *101*, 5583.
(33) Fukui, K. *J. Phys. Chem.* **1970**, *74*, 4161.
(34) Fukui, K. *Acc. Chem. Res.* **1981**, *14*, 363.
(35) Gonzales, C.; Schlegel, B. H. *J. Phys. Chem.* **1990**, *94*, 5523.
(36) Frisch, M. J.; Trucks, G. W.; Schlegel, H. B.; Gill, P. M. W.; Johnson, B. G.; Robb, M. A.; Cheeseman, J. R.; Keith, T.; Petersson, G. A.; Montgomery, J. A.; Raghavachari, K.; Al-Laham, M. A.; Zakrzewski, V. G.; Ortiz, J. V.; Foresman, J. B.; Cioslowski, J.; Stefanov, B. B.; Nanayakkara, A.; Challacombe, M.; Peng, C. Y.; Ayala, P. Y.; Chen, W.; Wong, M. W.; Andres, J. L.; Replogle, E. S.; Gomperts, R.; Martin, R. L.; Fox, D. J.; Binkley, J. S.; Defrees, D. J.; Baker, J.; Stewart, J. P.; Head-Gordon, M.; Gonzalez, C.; Pople, J. A. *Gaussian 94, Revision D.2*; Gaussian, Inc.: Pittsburgh, PA, 1995.
(37) Russell, S. T.; Warshel, A. *J. Mol. Biol.* **1985**, *185*, 389.
(38) Lee, F. S.; Chu, Z. T.; Warshel, A. *J. Comput. Chem.* **1993**, *14*, 161.
(39) Miertus, S.; Scrocco, E.; Tomasi, J. *Chem. Phys.* **1981**, *55*, 117.
(40) Miertus, S.; Tomasi, J. *Chem. Phys.* **1982**, *65*, 239.
(41) Pauling, L. *The Nature of the Chemical Bond*; Cornell University Press: Ithaca, NY, 1960.
(42) Florián, J.; Warshel, A. *ChemSol*; University of Southern California: Los Angeles, 1997.
(43) McQuarrie, D. A. *Statistical Mechanics*; Harper&Row: New York, 1976.
(44) Hwang, J. K.; King, G.; Creighton, S.; Warshel, A. *J. Am. Chem. Soc.* **1988**, *110*, 5297.
(45) Warshel, A. *Computer Modeling of Chemical Reactions in Enzymes and Solutions*; John Wiley & Sons: New York, 1991.
(46) Muller, R. P.; Warshel, A. *J. Phys. Chem.* **1995**, *99*, 17516.
(47) Warshel, A.; Russell, S. T. *Q. Rev. Biol.* **1984**, *17*, 283.
(48) Luzhkov, V. W., A. *J. Comput. Chem.* **1992**, *13*, 199.
(49) Warshel, A. *Biochemistry* **1981**, *20*, 3167.
(50) Gerlt, J. A.; Westheimer, F. H.; Sturtevant, J. M. *J. Biol. Chem.* **1975**, *250*, 5059.
(51) Guthrie, J. P. *J. Am. Chem. Soc.* **1977**, *99*, 3992.
(52) Benson, S. W. *J. Am. Chem. Soc.* **1958**, *80*, 5151.
(53) Ben-Naim, A.; Marcus, Y. *J. Chem. Phys.* **1984**, *81*, 2016.
(54) Cabani, S.; Gianni, P.; Mollica, V.; Lepori, L. *J. Solution Chem.* **1981**, *10*, 563.
(55) Blades, A. T.; Ho, Y. H.; Kebarle, P. *J. Am. Chem. Soc.* **1996**, *118*, 196.
(56) Florián, J.; Strajbl, M.; Warshel, A. Submitted.
(57) Fothergill, M.; Goodman, M. F.; Petruska, J.; Warshel, A. *J. Am. Chem. Soc.* **1995**, *117*, 11619.
(58) Hughes, E. D.; Ingold, C. K.; Shapiro, U. G. *J. Chem. Soc.* **1936**, 225.
(59) More O'Ferrall, R. A. *J. Chem. Soc. B* **1970**, 274.
(60) Jencks, W. P. *Chem. Rev. (Washington, D.C.)* **1972**, *72*, 705.
(61) Eyring, H.; Polanyi, M. *Z. Phys. Chem. B* **1931**, *12*, 279.
(62) Barnes, J. A.; Wilkie, J.; Williams, I. H. *J. Chem. Soc., Faraday Trans.* **1994**, *90*, 1709.
(63) Warshel, A.; Weiss, R. M. *J. Am. Chem. Soc.* **1980**, *102*, 6218.
(64) Mildvan, A. S. *Proteins* **1997**, *29*, 401.
(65) Pauling, L. *J. Am. Chem. Soc.* **1947**, *69*, 542.
(66) Barnard, P. W. C.; Bunton, C. A.; Llewellyn, D. R.; Oldham, K. G.; Silver, B. A.; Vernon, C. A. *Chem. Ind. (London)* **1955**, *760*, 2420.
(67) Butcher, W. W.; Wesheimer, F. H. *J. Am. Chem. Soc.* **1955**, *77*, 2420.
(68) Bunton, C. A.; Llewellyn, D. R.; Oldham, K. G.; Vernon, C. A. *J. Chem. Soc.* **1958**, 3574.
(69) Muller, R. P.; Florián, J.; Warshel, A. *NATO ASI* **1997**, *E342*, 47.
(70) Kumamoto, J.; Westheimer, F. H. *J. Am. Chem. Soc.* **1955**, *77*, 2515.
(71) Barnard, P. W. C.; Bunton, C. A.; Llewellyn, D. R.; Vernon, C. A.; Welch, V. A. *J. Chem. Soc.* **1961**, 2670.
(72) Kirby, A. J.; Varvoglis, A. G. *J. Am. Chem. Soc.* **1967**, *89*, 415.
(73) Stanton, R. E.; McIver, J. W., Jr. *J. Am. Chem. Soc.* **1975**, *97*, 3632.
(74) Williams, A. *Acc. Chem. Res.* **1989**, *22*, 387.
(75) Consider, for example, Figure 1 in ref 76, which shows a free energy surface for the nonenzymatic phosphoryl transfer reaction in such a way that the associative pathway has a 2 times higher activation barrier than the dissociative mechanism.
(76) Admiraal, S. J.; Herschlag, D. *Chem. Biol.* **1995**, *2*, 729.